Quaternary Science Reviews xxx (2010) 1–20

Contents lists available at ScienceDirect

Quaternary Science Reviews

journal homepage: www.elsevier.com/locate/quascirev

Paleoglaciological reconstructions for the Tibetan Plateau during the last glacial cycle: evaluating numerical ice sheet simulations driven by GCM-ensembles

Nina Kirchner [a,*], Ralf Greve [b], Arjen P. Stroeven [a], Jakob Heyman [a]

[a] Department of Physical Geography and Quaternary Geology, Stockholm University, 106 91 Stockholm, Sweden
[b] Institute of Low Temperature Science, Hokkaido University, Kita-19, Nishi-8, Kita-ku, Sapporo 060-0819, Japan

ARTICLE INFO

Article history:
Received 23 July 2010
Received in revised form
5 November 2010
Accepted 9 November 2010

ABSTRACT

The Tibetan Plateau is a topographic feature of extraordinary dimension and has an important impact on regional and global climate. However, the glacial history of the Tibetan Plateau is more poorly constrained than that of most other formerly glaciated regions such as in North America and Eurasia. On the basis of some field evidence it has been hypothesized that the Tibetan Plateau was covered by an ice sheet during the Last Glacial Maximum (LGM). Abundant field- and chronological evidence for a predominance of local valley glaciation during the past 300,000 calendar years (that is, 300 ka), coupled to an absence of glacial landforms and sediments in extensive areas of the plateau, now refute this concept. This, furthermore, calls into question previous ice sheet modeling attempts which generally arrive at ice volumes considerably larger than allowed for by field evidence. Surprisingly, the robustness of such numerical ice sheet model results has not been widely queried, despite potentially important climate ramifications. We simulated the growth and decay of ice on the Tibetan Plateau during the last 125 ka in response to a large ensemble of climate forcings (90 members) derived from Global Circulation Models (GCMs), using a similar 3D thermomechanical ice sheet model as employed in previous studies. The numerical results include as extreme end members as an ice-free Tibetan Plateau and a plateau-scale ice sheet comparable, in volume, to the contemporary Greenland ice sheet. We further demonstrate that numerical simulations that acceptably conform to published reconstructions of Quaternary ice extent on the Tibetan Plateau cannot be achieved with the employed stand-alone ice sheet model when merely forced by paleoclimates derived from currently available GCMs. Progress is, however, expected if future investigations employ ice sheet models with higher resolution, bidirectional ice sheet-atmosphere feedbacks, improved treatment of the surface mass balance, and regional climate data and climate reconstructions.

1. Introduction

The Tibetan Plateau is the highest and youngest plateau in the world and represents, with an area of approximately 2.5×10^6 km^2 at an average altitude of more than 4000 m above sea level, a topographic feature of extraordinary dimension on a global scale (Fig. 1A). Due to its particular location and extent, the Tibetan Plateau strongly impacts regional and global climate. It has been proposed, for example, that the uplift of the Tibetan Plateau in response to the Indian-Asian continental collision caused changes in the Asian monsoon dynamics, and that it initiated a global cooling trend which in turn triggered the onset of Quaternary climate oscillations (Molnar and England, 1990; Raymo and Ruddiman, 1992; Ramstein et al., 1997; An et al., 2001). As the uplift of the Tibetan Plateau resulted in regionally drier and colder conditions, it affected the inception, timing and extent of Quaternary glaciations on the plateau itself and enforced large-scale and profound environmental changes such as the formation of the Taklamakan and Badain Jirin Deserts bounding the Tibetan Plateau at its northern edge (Wu, 1981; Yang, 2000; Baosheng et al., 2001; Clark et al., 2004; Lehmkuhl and Owen, 2005).

The Tibetan Plateau region presently holds most glaciers outside the polar regions, with the largest ice covered areas in the Himalaya, Karakoram, Tien Shan, Pamir and Kunlun Shan (Dyurgerov and Meier, 2005; Fig. 1A). The number of glaciers in the Himalaya is estimated to lie between 12,000 and 15,000, with an additional 5000 glaciers in the Karakoram (Inman, 2010).

The glacial history of the Tibetan Plateau has been investigated for at least a hundred years. However, this history has received considerably less focus than for example the American and Eurasian North which hosted the Laurentide ice sheet and Fennoscandian ice

* Corresponding author. Tel.: +46 8 162988, +46 70 6090588; fax: +46 8 164818.
E-mail addresses: nina.kirchner@natgeo.su.se (N. Kirchner), greve@lowtem.hokudai.ac.jp (R. Greve), arjen.stroeven@natgeo.su.se (A.P. Stroeven), jakob.heyman@natgeo.su.se (J. Heyman).

0277-3791/$ – see front matter © 2010 Elsevier Ltd. All rights reserved.
doi:10.1016/j.quascirev.2010.11.006

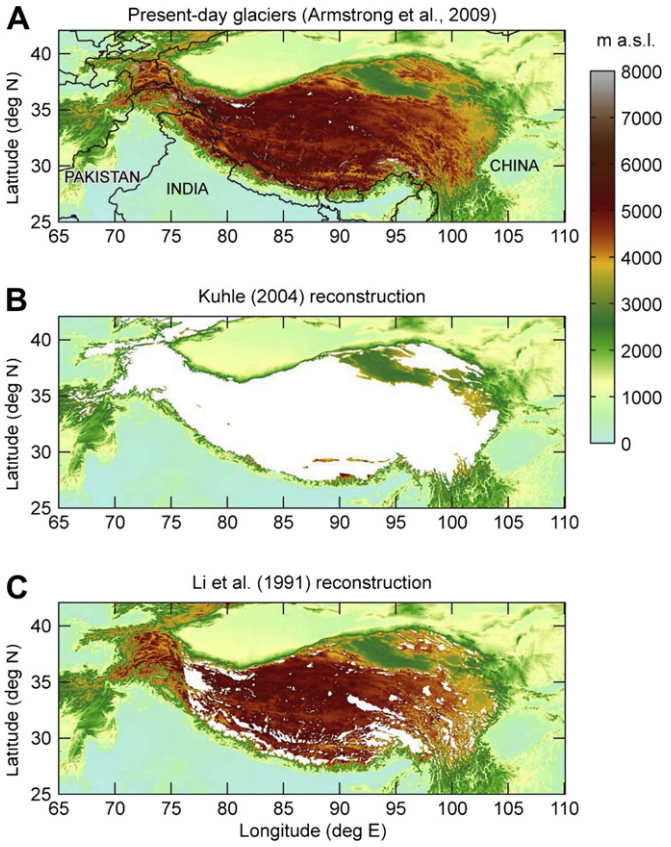

Fig. 1. Glaciations on the Tibetan Plateau. (A) Present day glaciers according to the GLIMS-data (Armstrong et al., 2009). (B) Spatial reconstruction of a plateau-scale ice sheet on the Tibetan Plateau as suggested by Kuhle (2004). (C) The moderate 'Quaternary' glacial reconstruction (Li et al., 1991) with glaciers covering approximately 22% of the plateau area which is above 2000 m asl.

sheet, respectively, during Quaternary glacial maxima (Kleman et al., 1997, 2002; 2010; Mangerud et al., 1998; Boulton et al., 2001; Knies et al., 2001; Dyke et al., 2002; Svendsen et al., 2004).

Two crucial knowledge gaps have stimulated an increased pace of research on the Tibetan Plateau over the past 30 years: the unknown maximum extent of Quaternary glaciation and the timing of glacial advances. Due to a scarcity of glacial geological data, spatial reconstructions of glaciations have diverged widely. For example, and arriving at an extreme reconstruction, Kuhle (1985, 1998, 2004, 2007) inferred the presence of a plateau-wide Tibetan ice sheet (of similar dimensions to the Greenland Ice Sheet; Fig. 1B) during the global Last Glacial Maximum. The ice sheet hypothesis is predominantly based on equilibrium line altitude (ELA) reconstructions. Because these are inferred to have fallen below the average plateau surface elevation, glaciation on a massif scale was inferred.

The Tibetan ice sheet reconstruction has received much criticism (cf Derbyshire et al., 1991; Rutter, 1995; Zheng and Rutter, 1998; Zhou et al., 2004; Lehmkuhl and Owen, 2005; Heyman et al., 2009). First, there is a notable absence of glacial landforms and sediments for extensive areas of the plateau. Typical glacial landforms in mountain regions include glacially eroded valleys and marginal moraines (e.g., Derbyshire et al., 1991; Zhou et al., 2004; Heyman et al., 2008; Stroeven et al., 2009), located in elevated mountain regions. These landforms are made by alpine-style valley glaciers and ice-fields/ice caps (Heyman et al., 2009). Extensive areas of the Tibetan Plateau away from the high mountains lack such glacial landforms and sediments. Moreover, there is a notable absence of landforms which are highly abundant in formerly glaciated areas of North America and Fennoscandia, and therefore typical of ice sheet glaciation (cf Hättestrand, 1998; Kleman and Hättestrand, 1999; De Angelis, 2007), such as large-scale drumlin swarms, eskers, and ribbed moraines (cf Heyman et al., 2008, 2009).

Second, the employed ELA extrapolation does not compensate for increasing aridity towards the interior of the plateau. Contemporary and former aridity gradients towards the central Tibetan Plateau result and have resulted in a rising of the ELA towards the interior thus counterbalancing the effect of depressed temperature on ELA (Lehmkuhl, 1998; Owen and Benn, 2005).

Finally, cosmogenic exposure and luminescence techniques have yielded a large number of exposure ages for moraines formed by local valley glaciers that are significantly older than the LGM and in some cases several hundred thousand years old (Schäfer et al., 2002, 2008; Chevalier et al., 2005; Owen et al., 2005, 2006a,b, 2009, 2010; Seong et al., 2009). These results clearly show that no plateau-scale ice sheet has existed on the Tibetan Plateau over at least the last glacial cycle (cf Schäfer et al., 2002; Owen et al., 2005, 2008).

In contrast to the Tibetan ice sheet reconstruction, several studies have presented maximum spatial reconstructions with former glaciers restricted to the highest mountain areas (Frenzel, 1960; Li et al., 1991; Shi et al., 1992). Li et al. (1991) presented a map of the maximum Quaternary (time-undefined) glacial extent for the Tibetan Plateau where glaciers only covered about one-fifth of the plateau area >2000 m asl (Fig. 1B). This reconstruction portrays ice masses slightly larger than the most extensive present-day ice caps (e.g., Barnes ice cap, Baffin Island). New field mapping using satellite imagery (e.g., Heyman et al., 2009; Moren et al., in review) and abundant cosmogenic exposure dating qualitatively supports the Li et al. (1991) maximum reconstruction and confirms that it predates the global LGM and, occasionally, even the entire last glacial cycle. In the absence of more recent and robust plateau-wide glacial reconstructions we accept the Li et al.' (1991) reconstruction (Fig. 1B), although diachronous in nature, as the best representation of maximum glacial extent. For more detailed data and reviews on the Tibetan Plateau glacial geology, see Derbyshire et al. (1991), Zheng and Rutter (1998), Lehmkuhl and Owen (2005), Owen et al. (2008), and Heyman et al. (2009).

Perhaps the strongest complementary approach to investigate the paleoglaciological history of the Tibetan Plateau is through numerical ice sheet modeling. Given realistic climate boundary conditions, ice sheet modeling has the potential to yield reconstructions with a resolution that can match field-based reconstructions. However, Pollard (2000) has shown that important limitations are imposed by knowing the climate boundary conditions. They use the output of 17 GCMs for three time periods, current, −6 ka and −21 ka, to compute ice extent and thickness for four domains (Greenland, Antarctica, glacial North America, and glacial Eurasia) after 10,000 years. The results show (Pollard, 2000; Fig. 14 therein) considerable differences in ice extent and thickness for current Greenland and ice age North America and Eurasia conditions even when just using the four highest-resolution GCMs available, at that time, in the Paleoclimate Modeling Intercomparison Project Phase 1 (PMIP1) database; http://pmip.lsce.ipsl.fr/. Based on the PMIP, which is currently in its third phase, a number of studies with off-line couplings between climate and ice sheet models have since then been performed (e.g. Abe-Ouchi et al., 2007; Charbit et al., 2007).

Crucial to the performance of any ice sheet model when conducting paleosimulations is the method of reconstructing past climate. Typically, an 'anomaly' approach combined with a glacial index function is employed in present ice sheet modeling (cf Section 2.3). The anomalies considered concern the surface air temperature field and the precipitation field, respectively. Temperature anomalies (with respect to present-day conditions) are given by the difference between present-day values and LGM values with appropriate

Please cite this article in press as: Kirchner, N., et al., Paleoglaciological reconstructions for the Tibetan Plateau during the last glacial cycle:..., Quaternary Science Reviews (2010), doi:10.1016/j.quascirev.2010.11.006

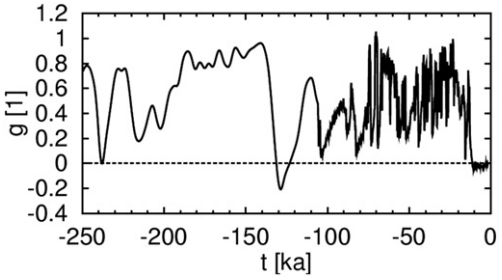

Fig. 2. Glacial index. Glacial Glacial index $g(t)$ as derived from the GRIP and Vostok surface temperature records (Dansgaard et al., 1993; Johnsen et al., 1995; Petit, 1999).

accounting of the orographic differences between a present-day ice mass and its LGM counterpart (cf eq. (4)). In contrast, precipitation anomalies are defined as a ratio (cf eq. (5)). Considering these anomalies, systematic errors in parameters affecting the modeling results are largely eliminated.

The glacial index function $g(t)$ is a measure for the climate state at any time t, obtained from, for example, synthetic blends of the $\delta^{18}O$ records from the Vostok ice core and the GRIP ice core (Dansgaard et al., 1993; Petit, 1999; Greve, 2005). Following Johnsen et al. (1995), the glacial index function is defined as:

$$g(t) = \frac{T_s(t) - T_{s,\text{present}}}{T_{s,\text{LGM}} - T_{s,\text{present}}}. \quad (1)$$

Obviously, $g = 1$ denotes glacial conditions, while $g = 0$ denotes present (interglacial) conditions (Fig. 2). Snapshots of the climatic fields at LGM and at present suffice to reconstruct the paleoclimatic inputs needed to drive the ice sheet model for 125 ka. The potential impact of the glacial index is discussed in Section 4.

Pollard (2000) refers to the anomaly approach as the 'perturbative delta method'. In their discussion of the methodology (Pollard, 2000, p. 103–104), they question whether the use of the delta method does indeed systematically reduce the uncertainty inherent in the GCM-based data entering the ice sheet simulations. They suspect that

> "it seems likely that the results of long-term coupled simulations with dynamic ice-sheet models would depend seriously and probably spuriously on the choice of one or another of these GCMs."

Indeed, the diversity of glacial reconstructions for the Tibetan Plateau from four ice sheet modeling studies support this statement. Three of these studies (Calov and Marsiat, 1998; Kuhle, 1998; Greve et al., 1999) were performed prior to Pollard's (2000) work and the fourth (Bintanja et al., 2002) does not include a comparison with Pollard (2000). Note that the support is by analogy, as Pollard (2000) does not investigate the Tibetan Plateau region specifically. For the Tibetan Plateau, Kuhle et al. (1989) presented the results of an ice sheet model forced by a lowering of the ELA to elevations below that of the plateau area. This procedure induced an ice sheet build-up within 10 ka, also with moderate precipitation. Calov and Marsiat (1998), Greve et al. (1999) and Bintanja et al. (2002) run numerical models designed to simulate the behavior of ice masses during glacial cycles on the entire Northern Hemisphere, thus also including results for the Tibetan Plateau. Calov and Marsiat (1998) and Greve et al. (1999) obtained, from their models, a complete ice cover over the Tibetan Plateau, while the Bintanja et al. (2002) model yielded extensive ice only for the southern margin of the Tibetan Plateau, considerably more extensive than geologically constrained spatial reconstructions (Li et al., 1991).

Suspected reasons for the poor performance of these numerical ice sheet model simulations is the limited spatial resolution of the Tibetan Plateau data, combined with insufficient complexity in the climate forcing and oversimplified or ignored treatment of possible feedback mechanisms, such as reduced albedo due to dust decomposition, in this area (Calov et al., 2005; Krinner et al., 2006). Thus, results from such simulations, and in light of the Pollard (2000) study, should be used with caution in comparison to spatial reconstructions.

The objective of this study is to systematically investigate the robustness of numerical modeling output for the Tibetan Plateau region, utilizing the Simulation Code for Polythermal Ice Sheets (SICOPOLIS) model (Greve, 2010). We present the glacial extents resulting from a large ensemble of GCM-derived climate forcings (90 members), the majority of which were extracted from the PMIP2-database (Braconnot et al., 2007; http://pmip2.lsce.ipsl.fr/pmip2/). With this set-up, we attempt to corroborate Pollard's (2000) hypothesis of a serious and perhaps spurious dependence of the simulated ice extents on the GCM employed.

2. Methods: ice sheet model and experimental design

2.1. The ice sheet model SICOPOLIS

SICOPOLIS is a 3D, thermodynamically coupled ice sheet model based on the Shallow Ice Approximation (Fowler and Larson, 1978; Hutter, 1982, 1993, 1983; Morland, 1984; Greve, 1997a) and is applicable to polythermal ice masses. The model has been benchmarked in a number of international ice sheet modeling intercomparison projects such as EISMINT and ISMIP-HEINO (Huybrechts et al., 1996; Calov and Greve, 2006; Calov et al., 2010). SICOPOLIS provides the time-dependent extent, thickness, velocity, temperature, water content and age for grounded ice sheets in response to external forcing. It employs the rheology of an incompressible, heat

Table 1
Standard physical parameters of the ice sheet model SICOPOLIS (Greve, 1997a, 2010), in SI or SI-derived units.

Quantity	Value
Acceleration due to gravity, g	9.81 m s^{-1}
Density of ice, ρ	910 kg m^{-3}
Exponent in Glen's flow law, n	3
Flow-enhancement factor in Glen's flow law, E	1 (Holocene ice)/3(Eemian ice)
Melting point at atmospheric pressure, T_0	273.15 K
Atmospheric lapse rate, γ_t	$-6.5 \cdot 10^{-3}$ K m^{-1}
Precipitation lapse rate, γ_p	$-0.001 \log(2.0)$ m^{-1}
Coefficient of heat conductivity (ice), κ	9.828 $e^{-0.0057T[K]}$ W m^{-1} K^{-1}
Specific heat of ice, c	$(146.3 + 7.253\,T\,[K])$ J kg^{-1} K^{-1}
Latent heat of ice, L	$335 \cdot 10^3$ J kg^{-1}
Clausius–Clapeyron gradient, β	$8.7 \cdot 10$ K m^{-1}
Isostatic time lag, τ_{iso}	94,670,856 s (3000 years)
Density of the astenosphere, ρ_a	3300 kg m^{-3}
Density × specific heat of the lithosphere, $\rho_r c_r$	$2000 \cdot 10^3$ J $m^{-3}K^{-1}$
Coefficient of heat conductivity (lithosphere), κ_r	3 W m^{-1} K^{-1}
Geothermal heat flux, q_{geo}	$55 \cdot 10^{-3}$ W m^{-2}
Factor of ice melt, β_2, in the PDD model	12 mm we d^{-1} °C^{-1} (default)/7 mm we d^{-1} °C^{-1} (reduced)
Factor of snow melt, β_1 (in the PDD model)	3 mm we d^{-1} °C^{-1}
Standard deviation of air temperature (in the PDD model)	5 °C
Saturation factor for the formation of superimposed ice in the PDD model	0.6

conducting power law fluid, commonly referred to as Glen's Flow Law, to describe the flow of ice. The thermomechanical coupling is described by the temperature- and water-content dependent rate factor suggested by Greve et al. (1998). Further, isostatic effects due to ice load are modeled by the Elastic-Lithosphere-Relaxing-Asthenosphere approach (Greve and Blatter, 2009). Apart from the isostatic adjustment, heat conduction in the lithosphere is the only other lithospheric process accounted for as it results in a thermal effect at the base of ice masses; it enters the simulations through the geothermal heat flux with its globally averaged value of $55 \cdot 10^{-3}\,\mathrm{W\,m^{-2}}$. Other standard parameters employed in SICOPOLIS are summarized in Table 1. More detailed information concerning SICOPOLIS can be found in Greve (1997a, 2010).

2.2. Spatio-temporal modeling domain, model resolution, basal topography

The modeling domain extends from 65°E to 110°E and from 25°N to 42°N (Fig. 1A) and straddles the entire Tibetan Plateau. It is discretized using a horizontal resolution of $1/12^\circ \times 1/12^\circ$, resulting in 541×205 in-plane (longitude/latitude) grid points. In the vertical, the cold ice column, the temperate ice layer and the lithosphere are discretized by 81, 11 and 11 grid points, respectively (Greve, 1997a).

The time span modeled comprises 125 ka: Simulations start with assumed initial ice-free conditions at $t = -125$ ka in the Eemian Interglacial associated with marine Oxygen Isotope Stage (OIS) 5e. The model evolves into the last glacial with maximal ice extents to be expected at OIS 4 at around −65 ka, and at the global LGM at −21 ka (OIS 2). Simulations end at 0 ka (present day). In the simulations, we use a fixed time step, which, however, ranges from $\Delta t = 1$ year (for runs with ice) to $\Delta t = 5$ years (for entirely ice-free runs).

The topography is derived from the contemporary ETOPO2v2 data set (U.S. Department of Commerce, NOAA, 2006). Note that by employing a present day topography, we assume that geological processes leading to changes in surface morphology and surface elevation have been negligible over the past 125 ka. Moreover, we assume that the topography represents the bedrock topography despite the fact that the ETOPO2v2 orogenic data represents the total elevation of the surface at a particular grid point, that is, includes, where applicable, contributions from non-zero ice thicknesses of ice masses. However, as today's glaciers on the Tibetan Plateau are confined to comparatively small geographical areas (Fig. 1A), the bias to slightly higher elevations is negligible for the paleosimulations performed here. Had we employed a coupled atmosphere-ice sheet model, in which ice masses – especially at high altitudes – may induce changes in the atmospheric circulation and hence in patterns of precipitation and temperature and therefore mass balance (Roe and Lindzen, 2001; Lindvall, 2009), the assumption of the ETOPO2v2 data representing the bedrock topography might become questionable.

2.3. Forcing of the Tibetan Plateau paleosimulations

The climate forcing required comprises the prescription of surface air temperature and precipitation. The reconstruction of past climate states is based on a decomposition of the (mean monthly) surface air temperature field into its present spatial pattern T^{present}, given as a function of longitude λ and latitude φ, and its time-dependent surface temperature variation δT_s, that is,

$$T(\lambda,\varphi,t) = T^{\mathrm{present}}(\lambda,\varphi) + \delta T_s(\lambda,\varphi,t). \tag{2}$$

The present-day temperature fields $T^{\mathrm{present}}(\lambda,\varphi)$ are taken from European Centre for Medium-range Weather Forecasting (ECMWF) from the years 1986–1989 and 1991–1994 (ECMWF, pers. communication, 1997), Legates and Willmott (1990a), and WorldClim (Hijmans et al., 2005). The comparatively old ECMWF and Legates and Willmott data sets ensure inter-comparability with previous SICOPOLIS simulations by Greve et al. (1999), Forsström et al. (2002) and Forsström and Greve (2004), while the WorldClim data provides forcing based on the newest generation of climate interpolations. In the following, the data sets will be abbreviated by 'ec', 'lw' and 'wclim'.

Past climate enters eq. (2) through different representations of $\delta T_s(\lambda,\varphi,t)$. A purely time-dependent representation of δT_s is obtained by relating $\delta T_s(t)$ to the δ^{18}O profile of the Greenland Ice Coring Project (GRIP) data (Dansgaard et al., 1993; Johnsen et al., 1995). In our modeling experiment, reconstructed temperatures from the GRIP core are available in time steps of 100 years, starting at −125 ka and ending at 0 ka. A linear interpolation scheme is used to infer temperatures at intermediate time steps. Reconstruction of former temperatures based on the GRIP data have been used previously, such as in simulations of the penultimate and last deglaciations of the Northern Hemisphere (Greve, 1997b; Greve et al., 1999). Because ice volumes over the Tibetan Plateau are overestimated in those simulations, we have included GRIP-based temperature reconstructions in our simulations to assess the effects of an alternative experimental set-up tailored specifically to the Tibetan Plateau area while the method of reconstructing temperatures through the past remains unchanged. In doing so, we can also investigate whether the GRIP forcing is perhaps more adequate when restrictively applied to the Tibetan Plateau area despite the fact that the Tibetan Plateau is located at a large distance from the source of the GRIP signal (Greenland) and has an extreme elevation and pronounced relief. In the ensemble runs, simulations in which former temperature distribution is obtained from the GRIP record are labeled 'grip' (Table 2).

Another representation of δT_s, which accounts for both temporal and spatial variations, is obtained from combining a glacial index function, $g(t)$, with LGM temperature anomalies derived from GCM's according to

$$\delta T_s(\lambda,\varphi,t) = g(t)\cdot T(\lambda,\varphi)^{\mathrm{GCM}}_{\mathrm{LGM-anom}}. \tag{3}$$

The glacial index function $g(t)$ is defined such that $g(t) = 1$ characterizes climatic conditions as observed at LGM, while $g(t) = 0$ mimics those observed at present (Dansgaard et al., 1993; Johnsen et al., 1995; Petit, 1999; Forsström and Greve, 2004). LGM temperature anomalies $T^{\mathrm{GCM}}_{\mathrm{LGM-anom}}$ are defined by

Table 2
The ensemble of climate forcings. Nine present-day temperature–precipitation scenarios, resulting from pairing three temperature sets (ECMWF, Legates & Willmott, and WorldClim) with three precipitation sets (Jaeger, Legates & Willmott, and WorldClim) are combined with 10 different paleoclimates (nine based on GCM anomalies, one based on the GRIP-record). The ensemble of climate forcings contains thus 90 members. On the basis of a numerical pre-study, the ECMWF data set as well as the GRIP paleoclimate is eventually considered inadequate for the purpose of modeling paleoglaciations on the Tibetan Plateau area. Hence, the final ensemble of climate forcings is reduced to $2 \times 3 \times 9 = 54$ members.

Temperature	Precipitation		
	Jaeger (1976)	Legates and Willmott (1990b)	WorldClim (Hijmans et al., 2005)
ECMWF (pers. comm.)	ec-jg-grip ec-jg-GCM	ec-lw-grip ec-lw-GCM	ec-wclim-grip ec-wclim-GCM
Legates and Willmott (1990a)	lw-jg-grip lw-jg-GCM	lw-lw-grip lw-lw-GCM	lw-wclim-grip lw-wclim-GCM
WorldClim (Hijmans et al., 2005)	wclim-jg-grip wclim-jg-GCM	wclim-lw-grip wclim-lw-GCM	wclim-wclim-grip wclim-wclim-GCM

Please cite this article in press as: Kirchner, N., et al., Paleoglaciological reconstructions for the Tibetan Plateau during the last glacial cycle:..., Quaternary Science Reviews (2010), doi:10.1016/j.quascirev.2010.11.006

$$T^{GCM}_{LGM-anom} = T^{GCM}_{LGM} - T^{GCM}_{present} - \gamma_t\left(h^{GCM}_{LGM} - h^{GCM}_{present}\right), \quad (4)$$

where T^{GCM}_{LGM} and $T^{GCM}_{present}$ denote the (GCM specific) temperature distribution at LGM and at present respectively, while $h^{GCM}_{LGM} - h^{GCM}_{present}$ accounts, in combination with the atmospheric lapse rate γ_t (cf Table 1) for changes in temperature attributable to changes in the surface elevation occurring between LGM and present. In the ensemble runs, simulations in which former temperature distributions as obtained from GCM anomalies are employed bear a generic label 'GCM' (Table 2).

Once the former surface air temperature fields are prescribed, former precipitation distributions are derived. For GRIP-based reconstructions, the precipitation field is related to the temperature variations $\delta T_s(t)$ in a linear manner. This linear relation involves a parameter γ_s chosen such that a 75% reduction in precipitation (as reconstructed from data from GRIP and GISP published by Dahl-Jensen et al. (1993), Cuffey and Clow (1997) and Alley (2000)) is obtained if a mean LGM surface temperature of $T = -17.5$ °C is considered; in doing so, the simulated ice volume at the LGM fits the sea-level low derived from the SPECMAP $\delta^{18}O$ record (Greve et al., 1999).

If $\delta T_s(\lambda,\varphi,t)$ is constructed using temperature anomalies as in eqns. (3) and (4), computation of former precipitation fields is achieved following (Greve, 2005) using today's precipitation values, the glacial index function $g(t)$ and precipitation anomalies $P_{LGM\text{-}anom}$ (note that the use of the exponential function is motivated by the Clausius–Clapeyron equation, stating that due to the saturation pressure of water vapour in the atmosphere, precipitation increases roughly exponentially with temperature):

$$\begin{aligned} P(\lambda,\varphi,t) &= P_{present}(\lambda,\varphi)\exp[g(t)\ln P_{LGM-anom}(\lambda,\varphi)] \\ &= P_{present}(\lambda,\varphi)\exp\left[g(t)\ln\frac{P^{GCM}_{LGM}}{P^{GCM}_{present}}(\lambda,\varphi)\right] \end{aligned} \quad (5)$$

Present day precipitation is obtained from Jaeger (1976), Legates and Willmott (1990b), and WorldClim (Hijmans et al., 2005). As was the case for the temperature data, the rather old data sets of Jaeger and Legates & Willmott are included to guarantee inter-comparability with previous simulations (Greve et al., 1999; Forsström et al., 2002; Forsström and Greve, 2004), while the WorldClim data represents the newest generation of forcing data available. In labeling the numerical simulations, we employ the abbreviations 'jg', 'lw' and 'wclim' to refer to these data sets; a detailed description of all data sets (temperature and precipitation) is given in Appendix A.

Conversion of mean monthly precipitation to mean monthly snowfall follows Marsiat (1994), implying that all precipitation is snow or rain, respectively, if mean monthly temperatures are below −10 °C or above 7 °C. For temperatures in between, a linear interpolation scheme is applied. Surface melting is parametrized by employing a Positive Degree Day (PDD) method with statistical temperature fluctuations, supplemented by the semi-analytic solution for the PDD integral (Braithwaite, 1984; Reeh, 1991; Calov and Greve, 2005), and rainfall is assumed to run off instantaneously. Further, SICOPOLIS accounts for ice sheet–atmosphere feedbacks through the atmospheric lapse rate γ_t, and an elevation-dependent precipitation lapse rate γ_p accounting for elevation desertification (Table 1).

2.4. The ensemble climate forcings

The ensemble of climate forcings comprises 90 individual forcings, resulting from combining nine different present-day temperature–precipitation scenarios (obtained from pairing three temperature data sets with three precipitation data sets) with 10 different paleoclimates (Table 2). Of those 10 paleoclimates, one is reconstructed on the basis of the GRIP record (Dansgaard et al., 1993; Johnsen et al., 1995), and the remaining nine are derived using GCM model output. In the ensemble of climate forcings, nine simulations have thus the acronym 'grip' in their generic label, while 81 contain an acronym specifying a particular GCM. The GCMs contributing to our forcing ensemble are listed in Table 3; the model output of seven of the GCMs was accessed through the PMIP2 database. The model output of the remaining two GCMs, namely the UKMO as a predecessor to the HadCM3M2 (Hewitt and Mitchell, 1997) and the LMDZ4 (Hourdin et al., 2006; Colleoni et al., 2009) was provided by personal communication (F. Colleoni). The GCM data was interpolated to the SICOPOLIS grid using a weighted, 2D linear interpolation. Paleoclimate reconstructions based on the GRIP data and the UKMO-data have been employed to force SICOPOLIS simulations by Forsström et al. (2002), Forsström and Greve (2004) and Greve et al. (1999), and are hence included to allow for an inter-comparability of model results and performance. The remaining eight paleoclimate-reconstructions are used as forcings to SICOPOLIS for the first time.

2.5. Screening of climate forcing ensemble members: a pre-study

To assess the individual climate forcing ensemble members' limitations when simulating the timing, extent and volume of glaciations on the Tibetan Plateau, different methods can be employed. One approach, not pursued here, is to perform a detailed analysis of the GCM model output data and of contemporary data sets for temperature and precipitation *prior* to using it to drive SICOPOLIS. As far as the GCM-reconstructed climates are concerned, much relevant information is contained in the PMIP2 database (Braconnot et al., 2007) where it awaits specification for the Tibetan Plateau region. Data sets providing the present-day climatology have been visually inspected (a detailed analysis is beyond the scope of this work); a short description is provided in Appendix A.

Table 3
Summary of the GCM's used to reconstruct the climate forcing in the SICOPOLIS runs. For each model, its acronym as used in the text is given, together with its full name and a reference where further documentation of the model is available. Moreover, the agency developing/maintaining/hosting the GCM is mentioned, as well as the database through which GCM model output has been accessed.

Acronym	Full name	Reference	Agency	Access
ccsm	CCSM3.0	http://www.ccsm.ucar.edu/publications/pub.info.html	NCAR; USA	PMIP2
cnrm	CNRM-CM33	http://www-pcmdi.llnl.gov/ipcc/model_documentation/CNRM-CM3.htm	MeteoFrance, CNRM; France	PMIP2
ecbil	ECBILT/CLIO	http://www.knmi.nl/onderzk/CKO/ecbilt.html	KNMI; Netherlands	PMIP2
fgoals	FGOALS-1.0g	http://www-pcmdi.llnl.gov/ipcc/model_documentation/FGOALS-g1.0.htm	LASG; China	PMIP2
had	HadCM3M2	http://pmip2.lsce.ipsl.fr/share/database/modeldocs/hadcm3m2/HadCM3M2.txt	MetOffice; UK	PMIP2
ipsl	IPSL-CM4	http://www-pcmdi.llnl.gov/ipcc/model_documentation/IPSL-CM4.htm	IPSL; France	PMIP2
miroc	MIROC3.2	http://www-pcmdi.llnl.gov/ipcc/model_documentation/MIROC3.2_medres.htm	CCSR/NIES/FRCGC; Japan	PMIP2
ukmo	UKMO	Hewitt and Mitchell (1997)	MetOffice; UK	pers. comm.
lmdz4	LMDZ4	Colleoni et al. (2009), Hourdin et al. (2006)	IPSL; France	pers. comm.

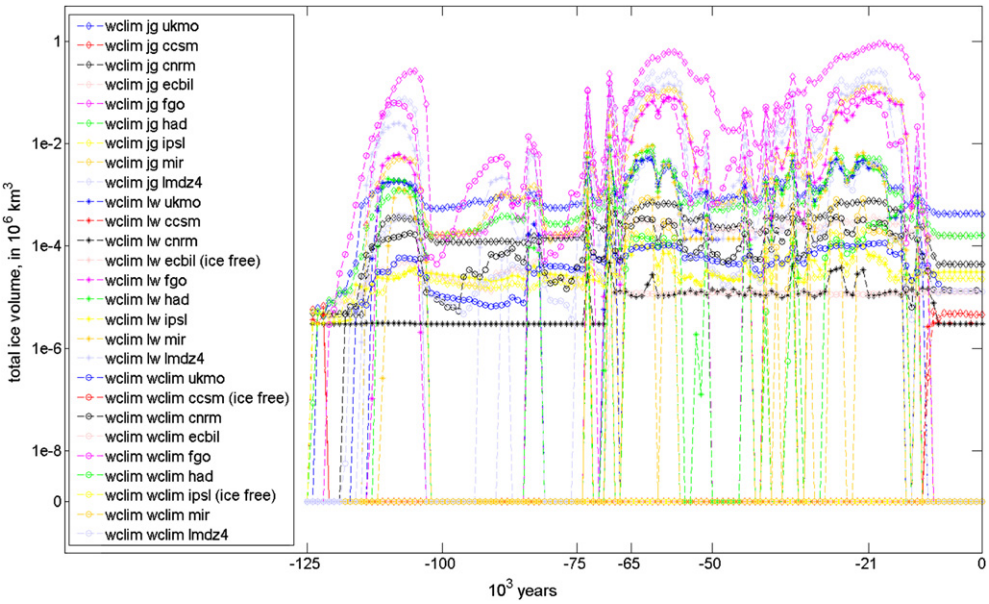

Fig. 3. Summary of the temporal evolution of total ice volumes over the Tibetan Plateau for 24 ensemble forcings providing numerical evidence for glaciations during the last 125 ka. Note that the simulated ice volumes range over six orders of magnitude, and that the individual climate forcings give rise to strikingly different glacial configurations at especially OIS4 and OIS2 (LGM). The figure is detailed in Figs. 4, 5 and 7 and 9. 30 ensemble forcing members yield ice-free conditions at all times: all forcings of type 'lw-xx-xx' (27, not plotted), and the forcings 'wclim-lw-ecbil', 'wclim-wclim-ccsm' and 'wclim-wclim-ipsl'. The factor for ice melt in the PDD model, β_2, is set to its default value of 12 mm we d^{-1} C^{-1}. Note that a semilogarithmic scale is employed on the vertical axis to ensure that low-ice volume runs remain detectable. On the horizontal axis, time t is marked using steps of 25 ka with two exceptions: time instance −25 ka is not plotted in favor of −21 ka (OIS2/LGM), and time instance −65 ka (OIS 4) is added.

Instead, we performed a numerical pre-study in which we assessed the performance of the combination of each GCM- and GRIP-derived forcing with today's temperature and precipitation by inspecting resulting glacial configurations over the Tibetan Plateau at three key time-slices: OIS 4, OIS2 (LGM), and today. If modeled ice extent during these time-slices obviously contradicts glacial geological evidence or current observations, either the method of reconstructing the climate (GRIP-based or GCM-based) or the data set containing contemporary temperature or precipitation were considered inadequate for modeling glaciations on the Tibetan plateau. Our pre-study comprised a full simulation of 125 ka for each of the 90 ensemble members, performed with a 10′ × 10′ and 20′ × 20′ grid resolution, respectively. As grid resolution increased from 20′ × 20′ to 10′ × 10′, ice volumes were observed to increase slightly, implying that the results from the pre-study runs underestimate the corresponding ice volumes computed eventually on the fine 5′ × 5′ grid used in the main study.

3. Results

We present the results of 54 paleoglaciological histories of the Tibetan Plateau during the last glacial cycle. These are the results of a reduced ensemble of climate forcings, while a reduction of 36 members resulted from the pre-study (cf Section 3.1 and Table 2). Fig. 3 displays a synoptical summary of the paleoglaciological evolution for those 24 members of the reduced ensemble which yielded non-vanishing total ice volumes (30 members of the ensemble forcing result in ice-free conditions during the entire last 125 ka). The simulated ice volumes range over six orders of magnitude in response to the ensemble of climate forcings, and give rise to strikingly different glacial configurations especially at OIS 4 and OIS 2 (LGM). Model results are grouped using ice volume as primary characteristic; we will discuss restricted (<60 km^3), moderate (<60 km^3–6000 km^3), large (6000 km^3–60000 km^3) and extensive (60,000 km^3–3,000,000 km^3) glaciations. The results will be detailed in the following sections.

3.1. Pre-study

On the basis of the pre-study we removed the ECMWF temperature data set from the ensemble of climate forcings. This decision was motivated by comparing observed glacial extents on the Tibetan Plateau (Fig. 1A) with modeling results for $t = 0$ (today) in runs involving the ECMWF data. A number of simulations 'ec-xx-xx' resulted in contemporary ice volumes in excess of 3 million km^3, that is, in excess of a Greenland Ice Sheet in its current configuration. Because there is at present no ice sheet over the Tibetan Plateau, we discarded the ECMWF-data set.

Past climate reconstructions based on the GRIP data were also discarded from the ensemble. This decision was motivated by comparing glacial configurations for simulations of the type 'ec-xx-grip' (cf Table 2), with glacial geologic evidence available for OIS 2 and OIS 4. Modeled ice volumes at OIS 4 were in the range of 4–5 million km^3 and at OIS 2 between 4,5 and 5,5 million km^3. However, the available glacial geologic evidence clearly does not support such extensive glaciations. Exposure dating and luminescence dating of glacial deposits have shown that during at least the last glacial cycle no plateau-scale ice sheet has existed on the Tibetan Plateau (Schäfer et al., 2002; Owen et al., 2005, 2008, 2009). Thus, we discarded the paleoclimate forcings derived from the GRIP record. We conclude that as a result of the pre-study, a reduced climate forcing ensemble of 54 members ($2 \times 3 \times 9$) should be used in the high-resolution runs, the results of which are presented in Section 3.2–3.6.

3.2. Ice-free Tibetan Plateau

Forcing SICOPOLIS with the 27 ensemble members of the type 'lw-xx-xx' results in entirely ice-free conditions during the last 125 ka. This is explained by the fact that the Legates and Willmott (1990a) temperatures provide the warmest summer temperatures of the climates considered here (Appendix A; Fig. A1). Remarkably, the effects of the contemporary Legates and Willmott surface air temperature are dominant to such an extent that variations in the

Please cite this article in press as: Kirchner, N., et al., Paleoglaciological reconstructions for the Tibetan Plateau during the last glacial cycle:..., Quaternary Science Reviews (2010), doi:10.1016/j.quascirev.2010.11.006

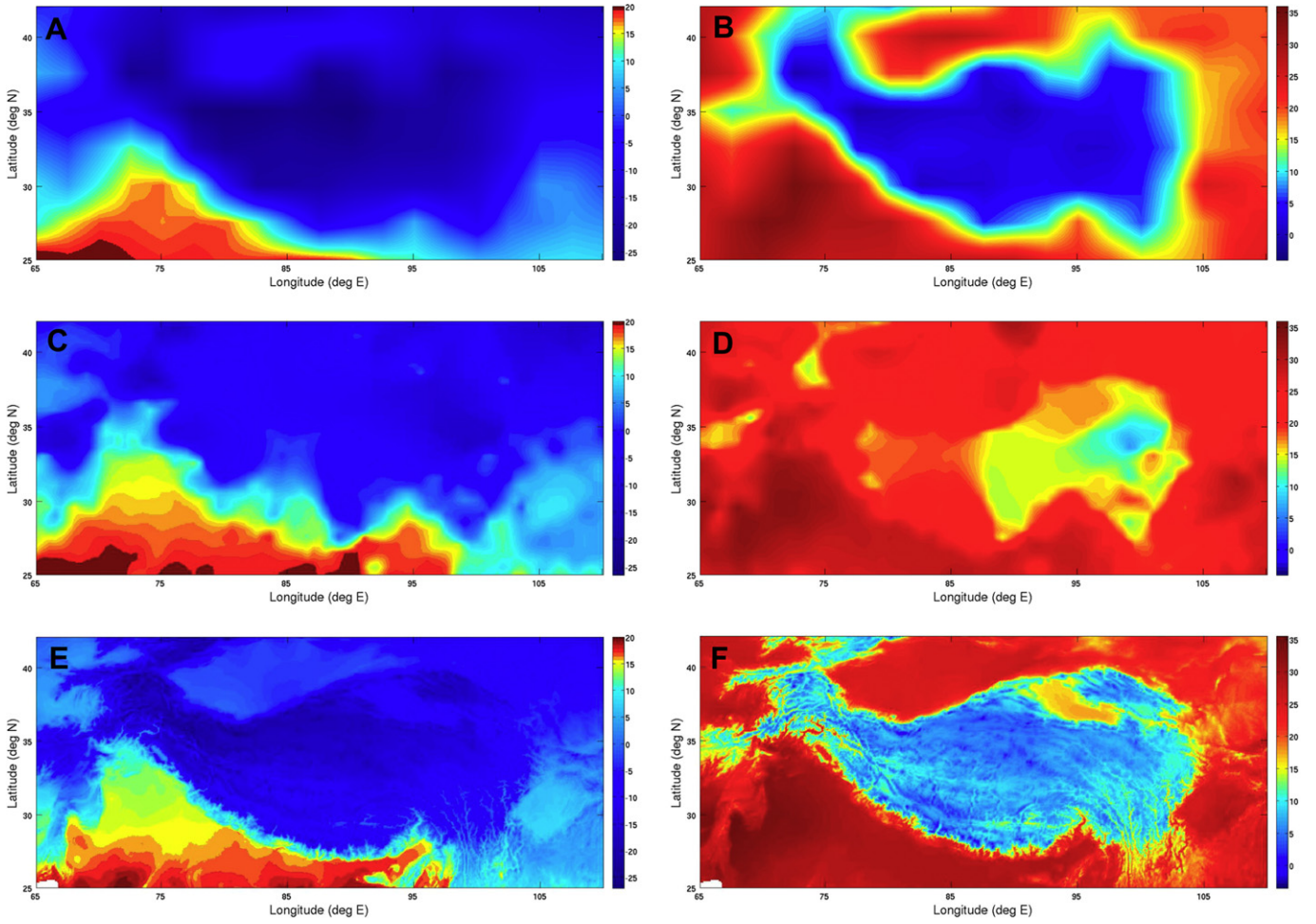

Fig. A1. Illustration of the contemporary temperature data sets used to force SICOPOLIS. (A) Contemporary February mean surface air temperatures over the Tibetan Plateau as derived from the ECMWF data set. (B) Contemporary August mean surface air temperatures over the Tibetan Plateau as derived from the ECMWF data set. (C) Contemporary February mean surface air temperatures over the Tibetan Plateau as derived from the Legates & Willmott data set. (D) Contemporary August mean surface air temperatures over the Tibetan Plateau as derived from the Legates & Willmott data set. (E) Contemporary February mean surface air temperatures over the Tibetan Plateau as derived from the WorldClim data set. (F) Contemporary August mean surface air temperatures over the Tibetan Plateau as derived from the WorldClim data set.

paleotemperatures as occurring from the use of different GCM reconstructions leave no footprint that is detectable using 'ice extent' or 'ice volume' as indicators.

To probe the dominance of the Legates and Willmott surface temperature data, we substituted the PDD factor for ice melt of 12 mm we (water equivalent) $d^{-1}\,{}^{\circ}C^{-1}$ default value of β_2 used earlier by, e.g., Greve et al. (1999), by $\beta_2 = 7$ mm we $d^{-1}\,{}^{\circ}C^{-1}$ (Table 1). In adopting this latter value we followed Zhang et al. (2006) who reported a mean value of $\beta_2 = 7.1$ mm we $d^{-1}\,{}^{\circ}C^{-1}$ based on measurements carried out on 15 glaciers on the Tibetan Plateau. Although decreasing the value of β_2 will lead to increasing ice volumes within the PDD method, the Legates and Willmott surface temperature data dominated over such possible effects induced by the variation in the melt factor for ice. Thus, all ensemble forcing members of type 'lw-xx-xx' yielded ice-free conditions during the entire 125 ka, irrespective of whether the melt factor for ice in the PDD model was assigned its default value or a lower one. A more rigorous sensitivity analysis allowing β_2 to range between 8.0 mm we $d^{-1}\,{}^{\circ}C^{-1}$ and 20.0 mm we $d^{-1}\,{}^{\circ}C^{-1}$ has recently been performed by Stone et al. (2010) who used Latin hypercube sampling to evaluate the equilibrium ice volume of the Glimmer-CISM ice sheet model for Greenland under modern climatology.

The three ensemble forcing members 'wclim-lw-ecbil', 'wclim-wclim-ccsm' and 'wclim-wclim-ipsl' give rise to ice-free conditions during the entire 125 ka in runs where the PDD factor for ice melt, β_2, is set to is default value. However, for these three members, the interplay of present-day climatology and reconstructed past climates is sensitive to a decrease in β_2 such that the Tibetan Plateau features glaciations of different extents when the reduced value for β_2 is used. The forcing members 'wclim-wclim-ccsm' and 'wclim-wclim-ipsl' then give rise to restricted ice volumes (<60 km^3), while the forcing 'wclim-lw-ecbil' results in moderate ice volumes (60 km^3–6000 km^3) over the Tibetan Plateau. The ice volume time series in response to 'wclim-wclim-ccsm' and 'wclim-wclim-ipsl' are therefore included in Fig. 4 (see Section 3.3), and for 'wclim-lw-ecbil' in Fig. 5 (see Section 3.4).

3.3. *Restricted glaciation (<60 km^3)*

Irrespective of which value for the ice melt factor is used, small total ice volumes (<60 km^3) over the Tibetan Plateau are obtained from three forcings: 'wclim-jg-ccsm', 'wclim-lw-ccsm' and 'wclim-wclim-ecbil'. In all three cases, ice volumes resulting from runs with the reduced ice melt factor β_2 are larger than those obtained from runs with the default ice melt factor. The timing and duration of glaciations in response to a particular forcing are not significantly affected by the value of the ice melt factor (Fig. 4), as each two time series for a fixed forcing but with different values of β_2 indicate

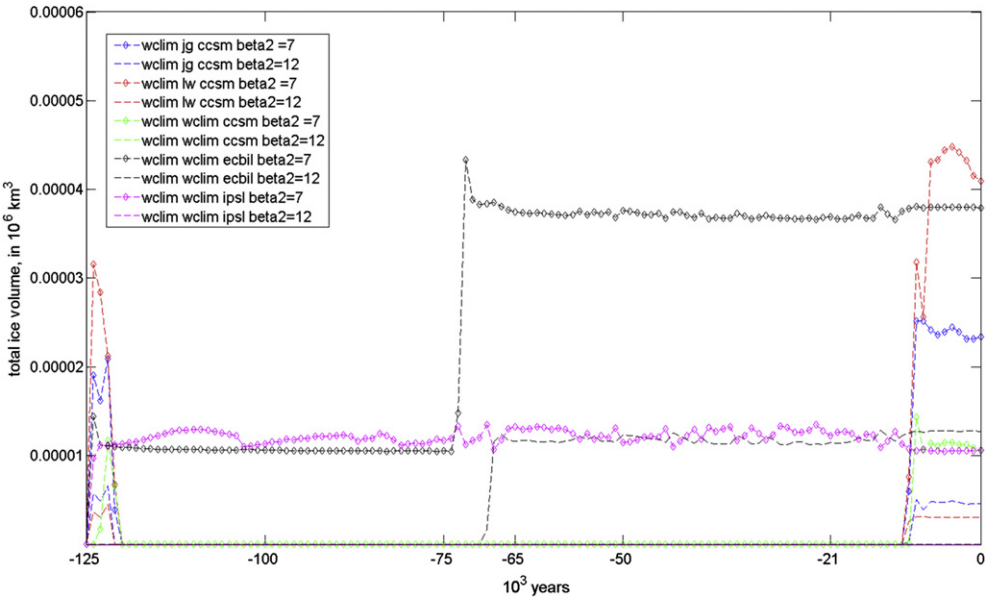

Fig. 4. Temporal evolution of small (<60 km^3) total ice volumes over the Tibetan Plateau. Small total ice volumes as modeled in response to three forcings from the ensemble ('wclim-jg-ccsm', 'wclim-lw-ccsm' and wclim-wclim-ecbil') and for different choices of the ice melt factor β_2 in the PDD model. It is seen that the GCM used in the reconstruction of the paleoclimates determines the onset and the timing of glaciations, for details see Section 3.3.

through relatively synchronous behavior. However, the onset and duration of glaciations are strongly affected by the choice of the GCM from which the paleoclimate is derived. Ice volumes in response to forcing 'ecbil', on the one hand, peak right before OIS 4 and remain essentially unchanged from −70 ka onward, yielding the modeled presence of small contemporary glaciers on the Tibetan Plateau. Ice volumes in response to forcing 'ccsm', on the other hand, are characterized by an absence of ice during the entire last glacial (including the LGM) except for the Holocene. Here, an onset of glaciation is detected at about −10 ka and at two different geographical locations: forcings 'wclim-jg-ccsm' and 'wclim-lw-ccsm' result in an ice covered area located approximately at the geographical position of Mt. Everest, 86°E, 28°N.

Forcings 'wclim-wclim-ccsm' and 'wclim-wclim-ipsl' give rise to small ice volumes only if a reduced factor for ice melt is employed (these runs are ice-free if the default value for β_2 2 is used, cf Section 3.2). The time series of the corresponding ice volume evolution is included in Fig. 4. Ice volume evolution, in particular onset of glaciation, in response to forcing 'wclim-wclim-ccsm' is synchronous to the ones observed for the other 'ccsm' runs: ice-free conditions throughout the major part of the last glacial cycle, including especially ice-free conditions at OIS 2, and onset of

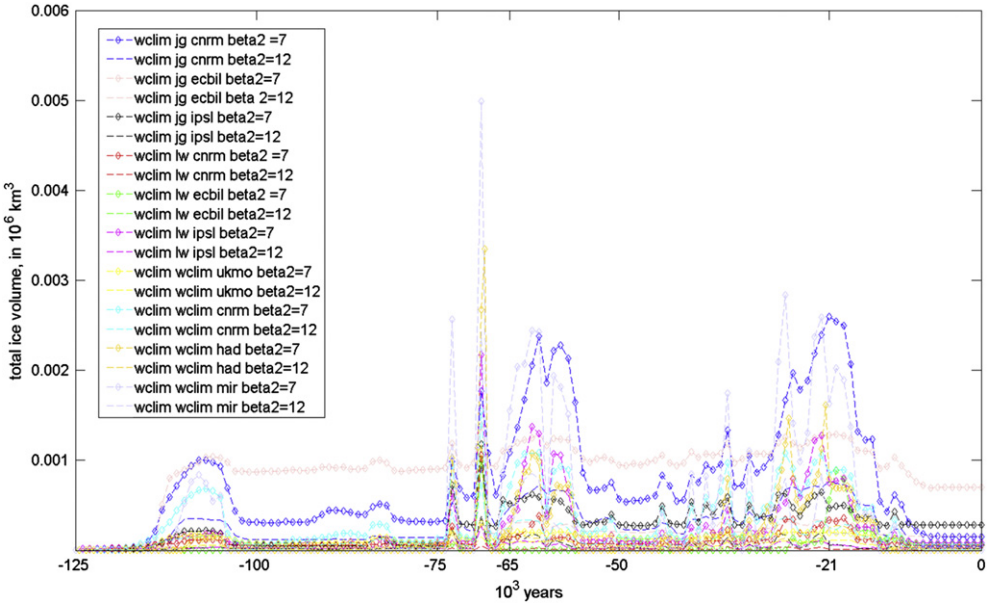

Fig. 5. Temporal evolution of medium (60 km^3–6000 km^3) total ice volumes over the Tibetan Plateau. Medium total ice volumes as modeled in response to 10 forcings from the ensemble and for different choices of the ice melt factor β_2 in the PDD model: Note the highly variable ice volumes around OIS4 for which some glacial configurations exceed their counterparts attained around OIS2 (LGM), for details, see Section 3.4.

Please cite this article in press as: Kirchner, N., et al., Paleoglaciological reconstructions for the Tibetan Plateau during the last glacial cycle:..., Quaternary Science Reviews (2010), doi:10.1016/j.quascirev.2010.11.006

glaciation around −10 ka. In contrast, the onset and timing of glaciation resulting from a paleoclimate derived on the basis of the 'ipsl' model is strikingly different because of a continuous persistence of ice patches through the entire glacial cycle.

3.4. Moderate glaciation (60 km^3–6000 km^3)

Irrespective of which of the two factors of ice melt is used, moderate total ice volumes (60 km^3–6000 km^3) over the Tibetan Plateau are obtained from nine forcings: 'wclim-jg-cnrm', 'wclim-jg-ecbil', 'wclim-jg-ipsl', 'wclim-lw-cnrm', 'wclim-lw-ipsl', 'wclim-wclim-ukmo', 'wclim-wclim-cnrm', 'wclim-wclim-had', and 'wclim-wclim-mir' (Fig. 5). Glaciation remains restricted to the mountain chain bordering the Tibetan Plateau to the south (in response to forcings involving contemporary Jaeger and Legates & Willmott precipitation data, respectively), the high-latitude north-northeastern part of the Plateau (in response to contemporary WorldClim precipitation data), and the northwestern central part of the Plateau (for forcings involving contemporary Jaeger precipitation data). The time series illustrate that the variability in total ice volume around OIS 4 is much larger than around OIS 2, and that the timing of maximum ice volume is governed by the choice of the GCM used in the climate reconstruction. For example, glaciation resulting from the forcing 'wclim-wclim-mir' attains its maximum LGM-volume earlier than 'wclim-jg-cnrm' does. Fig. 6 portrays the location and spatial extent of ice masses resulting for each of these nine simulations at OIS 4 and OIS 2, adopting the reduced factor of ice melt, β_2. For OIS 4 (Fig. 6A), maximum ice coverage is obtained

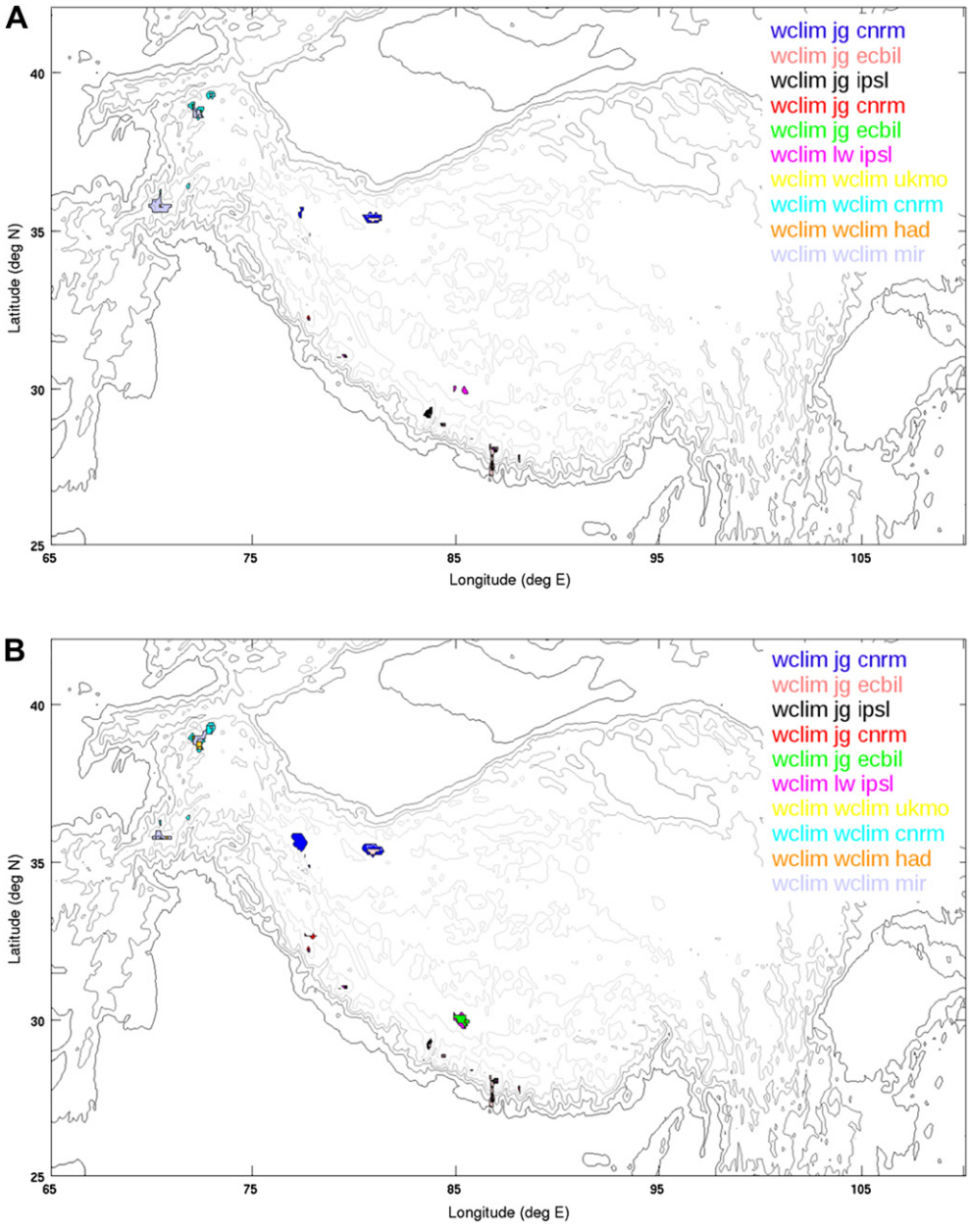

Fig. 6. The geographical location and spatial extents of medium sized Tibetan Plateau glaciations at OIS 4 (−65 ka, panel A) and OIS 2 (LGM, −21 ka, panel B). 10 ensemble forcing members give rise to overall medium ice volumes during the last 125 ka. The plot shows the spatial extents and geographical location of these ice volumes. Note that to enhance visibility of the results, the latter are plotted only for the simulations in which the reduced factor ice melt (giving rise to larger ice volumes) has been employed. The colors used correspond to those of Fig. 5, for details, see Section 3.4.

Please cite this article in press as: Kirchner, N., et al., Paleoglaciological reconstructions for the Tibetan Plateau during the last glacial cycle:..., Quaternary Science Reviews (2010), doi:10.1016/j.quascirev.2010.11.006

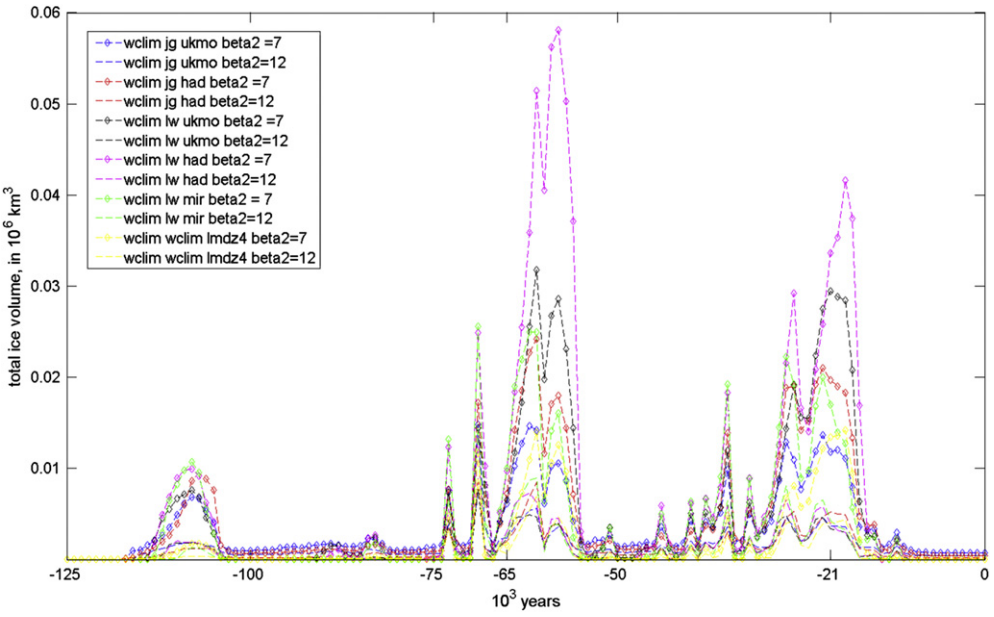

Fig. 7. Temporal evolution of large total ice volumes (6000 km^3–60,000 km^3) over the Tibetan Plateau. Large total ice volumes as obtained in response to 6 forcings from the ensemble, and for different choices of the ice melt factor β_2 in the PDD model. Note the large variability in total volumes of Tibetan Plateau glaciations as resulting from the different forcings.

from the forcing 'wclim-wclim-mir' (pale blue; cf also Fig. 5), and the pale blue patches located at roughly 70°E, 36°N indicate that for this forcing the OIS 4 glacial extent is larger than its corresponding OIS 2 (LGM) extent. The same is observed for 'wclim-jg-ipsl' (black patches), while for the remaining ensemble of forcing members, LGM ice extents are always large than their corresponding OIS 4 ice extents.

The forcing 'wclim-lw-ecbil' yields moderate ice volumes at two time slices, provided the ice melt factor β_2 is set to its reduced value (runs with the standard value are ice free; Section 3.2). Model results indicate ice volumes of 1000 km^3 lasting for roughly 3 ka–5 ka prior to OIS 4, and for approximately 15 ka around OIS 2, with ice-free conditions between these events. As with the other two forcing members showing distinct responses (ice free/ice cover) in response to variations in β_2, we conclude that the interplay of present-day climate and past climate is sensitive to decreases in the PDD factor for ice melt. Because the ice volumes used to group the results into restricted/moderate/large/extensive ice volume runs were set arbitrarily by us, we cannot conclude that the forcing member 'wclim-lw-ecbil' is more sensitive to changes in β_2 than the forcing members 'wclim-wclim-ccsm' and 'wclim-wclim-ipsl' (cf Sections 3.2 and 3.3).

3.5. Large glaciation (6000 km^3–60,000 km^3)

Generally, modeled volumes larger than 6000 km^3 are affected by changes in the ice melt factor β_2, however, not to such an extent that ice-free conditions result if the default value of β_2 is employed. Large total ice volumes over the Tibetan Plateau are obtained from 6 forcing members (and for both values of β_2): 'wclim-jg-ukmo', 'wclim-jg-had', 'wclim-lw-ukmo', 'wclim-lw-had', 'wclim-lw-mir' and 'wclim-wclim-lmdz4'.

In the temporal evolution of the six model runs resulting in large ice volumes (Fig. 7), it is observed that the maximum ice volume is occurring at OIS 4 for 'wclim-lw-had', and that this modeled OIS 4 ice volume is larger than its corresponding OIS 2 ice volume. Variability in overall ice volume remains high. In contrast to Fig. 5, the timing of the glaciations appears however more synchronous that in the case of the medium ice volume runs, as the ice volume time series for the forcing 'wclim-lw-had' acts as a bounding hull for all other ice volume time series. Despite this, individual ice volume evolutions differ considerable both in timing, duration and size.

To illustrate the modeled spatial extents of the large glaciations for both values of ice melt, we present OIS 2 (LGM) configurations from forcing members 'wclim-lw-had' and 'wclim-wclim-lmdz4' (Fig. 8A), OIS 2 (LGM) configurations from forcing members 'wclim-jg-ukmo' and 'wclim-lw-ukmo' (Fig. 8B), and OIS 4 configurations from forcing members 'wclim-lw-mir' and 'wclim-jg-had' (Fig. 8C). The primary location of ice caps that persist at both OIS 4 and OIS 2 are similar. However, their spatial extents vary due to disintegration of ice caps into smaller sized mountain glaciers (whenever OIS 4 volumes are larger than OIS 2 volumes), or to merging of smaller sized mountain glaciers into a coherent ice cap (whenever OIS 4 volumes are smaller than OIS 2 volumes). Likewise, the extent of the ice caps is affected by a change in the value of ice melt in the PDD model.

South of 34°N, local ice caps form along the mountain range bordering the Tibetan Plateau in response to precipitation forced by the contemporary Legates and Willmott data set, that is, for runs 'wclim-lw-xx'. Among the three runs of the type 'wclim-lw-xx' resulting in large ice volumes, paleoclimates 'had' and 'mir' result in ice caps restricted to the mountain range bordering the Tibetan Plateau to the south, while additional small and widely scattered ice caps in the north-northwestern to Central Tibetan Plateau north of 35°N are modeled in response to the 'ukmo' paleoclimate, that is, in the 'wclim-lw-ukmo' run. These scattered ice caps disappear if the Legates and Willmott precipitation data set is replaced by the one of Jaeger (1976), leaving only ice caps in the southern mountain range for the forcing 'wclim-jg-ukmo'. Replacing 'ukmo' by 'had' results in additional ice caps in the North–Northwest part of the Tibetan Plateau and a pronounced outlet glacier at approx 86°E, cf forcing 'wclim-jg-had'. Finally, the forcing 'wclim-wclim-lmdz4' results in ice caps along the southern mountain range, in isolated caps in the central part of the Plateau as well as in the high latitudes of the northwestern most part of the Tibetan Plateau.

Please cite this article in press as: Kirchner, N., et al., Paleoglaciological reconstructions for the Tibetan Plateau during the last glacial cycle:..., Quaternary Science Reviews (2010), doi:10.1016/j.quascirev.2010.11.006

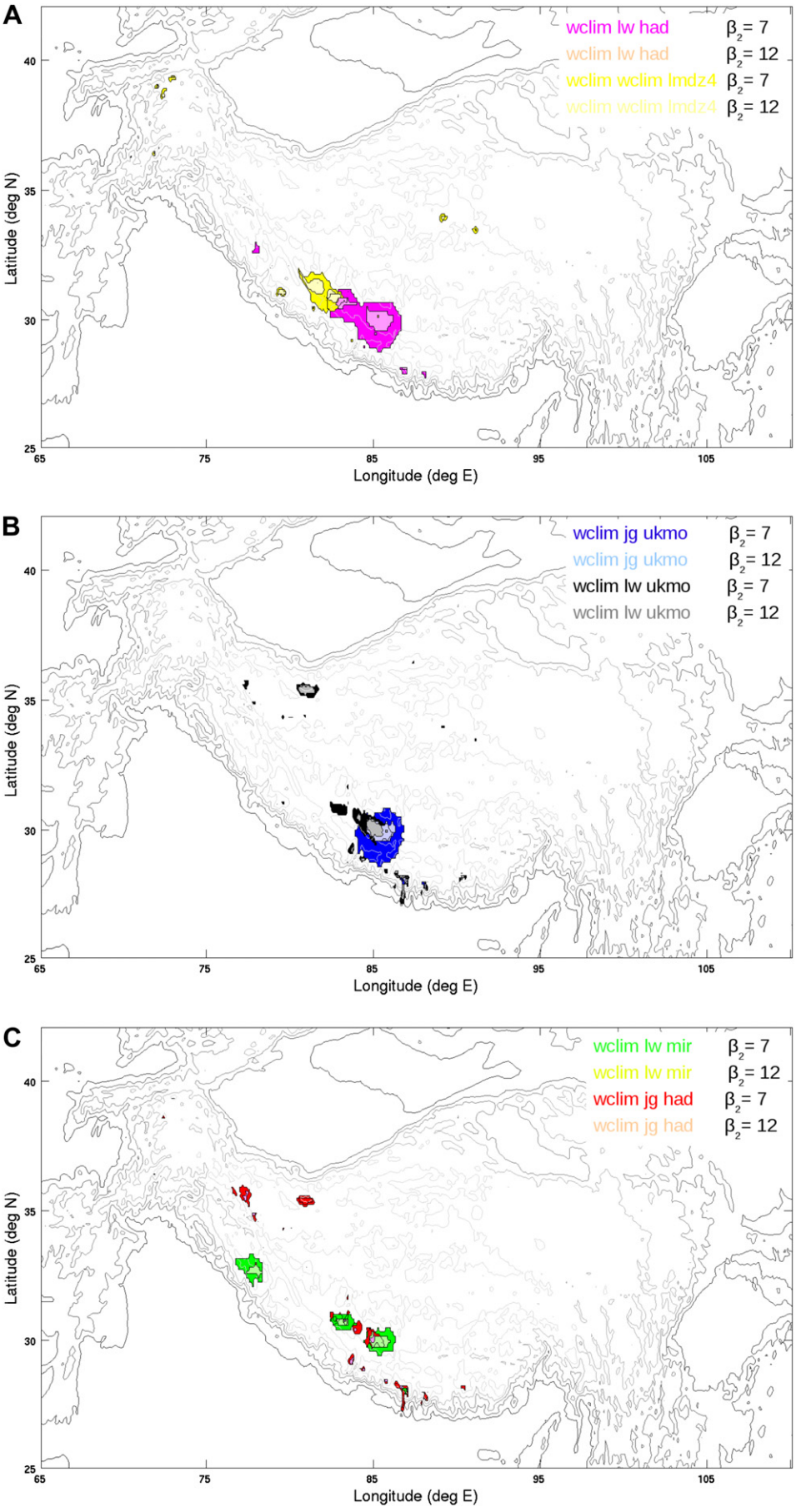
A
wclim lw had β2= 7
wclim lw had β2= 12
wclim wclim lmdz4 β2= 7
wclim wclim lmdz4 β2= 12
Latitude (deg N)
Longitude (deg E)
B
wclim jg ukmo β2= 7
wclim jg ukmo β2= 12
wclim lw ukmo β2= 7
wclim lw ukmo β2= 12
Latitude (deg N)
Longitude (deg E)
C
wclim lw mir β2= 7
wclim lw mir β2= 12
wclim jg had β2= 7
wclim jg had β2= 12
Latitude (deg N)
Longitude (deg E)

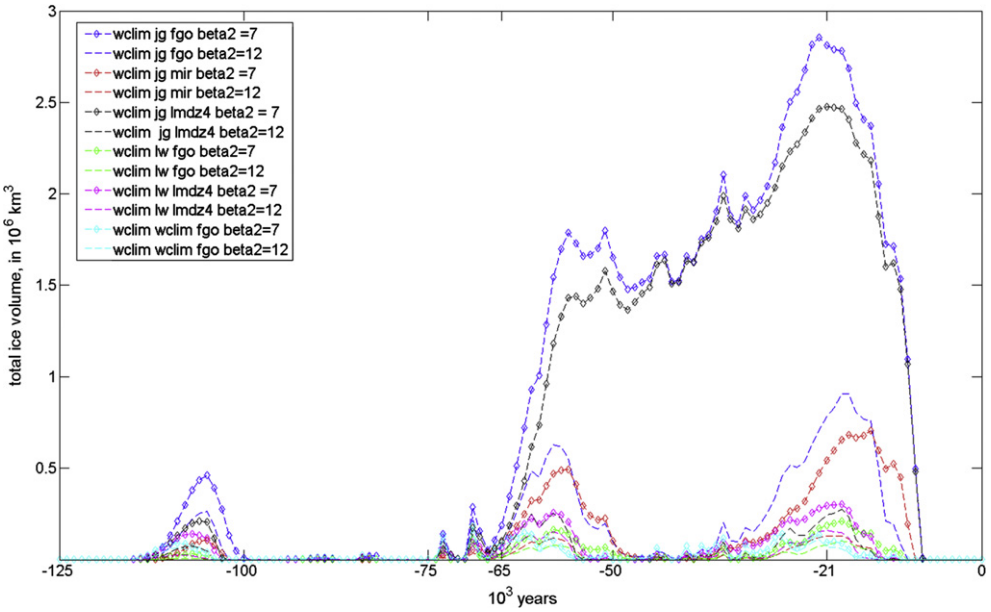

Fig. 9. Temporal evolution of extra-large total ice volumes (60,000 km^3–3,000,000 km^3) over the Tibetan Plateau. Modeled ice volume evolution for the six ensemble forcing members that give rise to extra-large ice volumes (for both values of β_2). Note the large variability in total volumes of Tibetan Plateau glaciations as resulting from the different forcings.

3.6. *Extensive glaciation (60,000 km^3–3,000,000 km^3)*

Extensive glaciations characterized by extra large total ice volumes, ranging in size in response to different values of the ice melt factors are obtained from six forcing members: 'wclim-jg-fgo', 'wclim-jg-mir', 'wclim-jg-lmdz4', 'wclim-lw-fgo', 'wclim-lw-lmdz4', and 'wclim-wclim-fgo' (Fig. 9). Modeled peak glaciations occur around OIS 4 and OIS 2 with maximal ice volumes up to 800,000 km^3 observed for runs in which the default ice melt factor β_2 is employed. If the reduced value of β_2 is used, however, ice volumes increase to 2,4 million km^3 and 3 million km^3 in response to forcing members 'wclim-jg-lmdz4' and 'wclim-jg-had', respectively. These forcing members result also in a continuous glaciation from −65 ka to −10 ka. It is worth noting that modeled ice volumes at OIS 2 are always larger than their OIS 4 counterparts, irrespective of whether continuous or discontinuous glaciation prevails.

The spatial extents of the glaciated areas at OIS 4 for the individual forcing members and for both values of ice melt are shown in Fig. 10. Inline with observations made for large glaciations (cf Section 3.5), forcing members using the contemporary Legates and Willmott precipitation data set yield ice caps along the mountain range bordering the Tibetan Plateau to the south. Likewise, forcing members using the contemporary 'wclim' precipitation data set yield ice caps in the high-latitude north–northwestern corner of the Tibetan Plateau. Model results indicate a number of ice caps in the northwestern and central parts of the Tibetan Plateau in response to forcing members using the 'jg' precipitation data set. For 'wclim-jg-mir' the model results are particularly sensitive to the value for ice melt. Individual ice caps merge into one coherent one if the reduced value of ice melt is employed. Spatial extents of ice sheets and ice caps at OIS 4 and OIS 2 (for both values of the ice melt factor) vary but occur in similar locations (Fig. 11). We interpret this to mean that modeled OIS 4 ice caps are also the centers/nuclei to the OIS 2 ice caps. At OIS 2, considerable areas are ice covered, particularly on the central western Tibetan Plateau and in its high-latitude northwestern corner.

4. Discussion

The aim of this work was to contrast timing, extent and duration of former glaciations on the Tibetan Plateau as indicated by glacial geology with those resulting from numerical ice sheet modeling. While modeling efforts coupled to glacial geological reconstructions have been previously employed for other formerly glaciated areas (such as for the Laurentide and Eurasian ice sheets, Howell et al., 1999; Kleman et al., 2002; Napieralski et al., 2007), this has never been attempted for the Tibetan Plateau. Especially intriguing is the fact that ice sheet models for the Northern Hemisphere that capture the overall behavior of the Laurentide and Eurasian ice sheets produce large ice masses over the Tibetan Plateau; a feature which has not been supported by geological data (Owen et al., 2005; Heyman et al., 2009).

None of the modeled ice masses (Figs. 3–11) matches the glacial geological record of the Tibetan Plateau when comparing the OIS 4 and OIS 2 ice extents with field evidence. Regarding the timing of glaciation, most of the 24 'glacial' model runs yielded their most extensive glaciers during OIS 2. This result is not supported by chronological evidence for past glaciations in Tibet. On the contrary, the paleoglaciological record reveals increasingly more extensive glaciation further back in time and most restricted glaciations during OIS 2 (Derbyshire et al., 1991; Schäfer et al., 2002; Lehmkuhl and Owen, 2005; Owen et al., 2005, 2008, 2009, 2010). Focusing on the spatial distribution, the models tend to produce more glaciers covering larger tracts of land in the western half than in the eastern half of the Tibetan Plateau, quite in contrast with glacial geological evidence (e.g., Li et al., 1991; Lehmkuhl and

Fig. 8. Spatial extents and geographical location of large ice volumes (6000 km^3–60,000 km^3) over the Tibetan Plateau. Six ensemble forcing members give rise to large ice volumes. (A) Ice extent at LGM (−21 ka) in response to forcing 'wclim-lw-had' and 'wclim-wclim-lmdz4'. (B) Ice extent at LGM (−21 ka) in response to forcings 'wclim-jg-ukmo' and 'wclim-lw-ukmo'. (C) Ice extent at OIS 4 (−65 ka) in response to forcings 'wclim-lw-mir' and 'wclim-jg-had'.

Please cite this article in press as: Kirchner, N., et al., Paleoglaciological reconstructions for the Tibetan Plateau during the last glacial cycle:..., Quaternary Science Reviews (2010), doi:10.1016/j.quascirev.2010.11.006

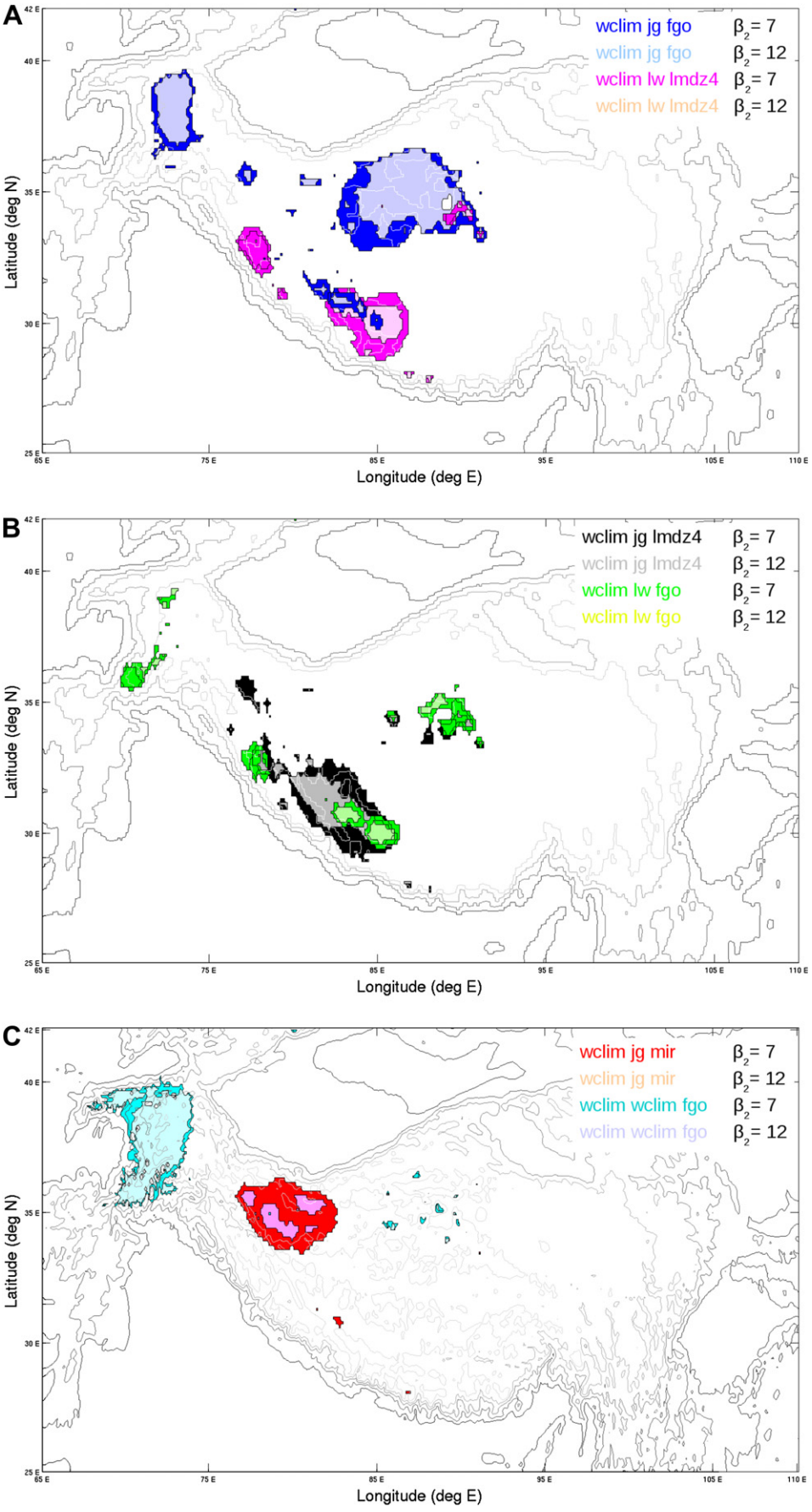

Fig. 10. Spatial extents and geographical location of extra-large ice volumes (60,000 km^3–3,000,000 km^3) over the Tibetan Plateau at OIS 4. (A) Modeled ice extent in response to forcings 'wclim-jg-fgo'and 'wclim-lw-lmdz4'. (B) Modeled ice extent in response to forcings 'wclim-jg-lmdz4' and 'wclim-lw-fgo'. (C) Modeled ice extent in response to forcings 'wclim-jg-mir' and 'wclim-wclim-fgo'. For a comparison of the OIS4 ice extents to their OIS2 counterparts, see Fig. 11.

Please cite this article in press as: Kirchner, N., et al., Paleoglaciological reconstructions for the Tibetan Plateau during the last glacial cycle:..., Quaternary Science Reviews (2010), doi:10.1016/j.quascirev.2010.11.006

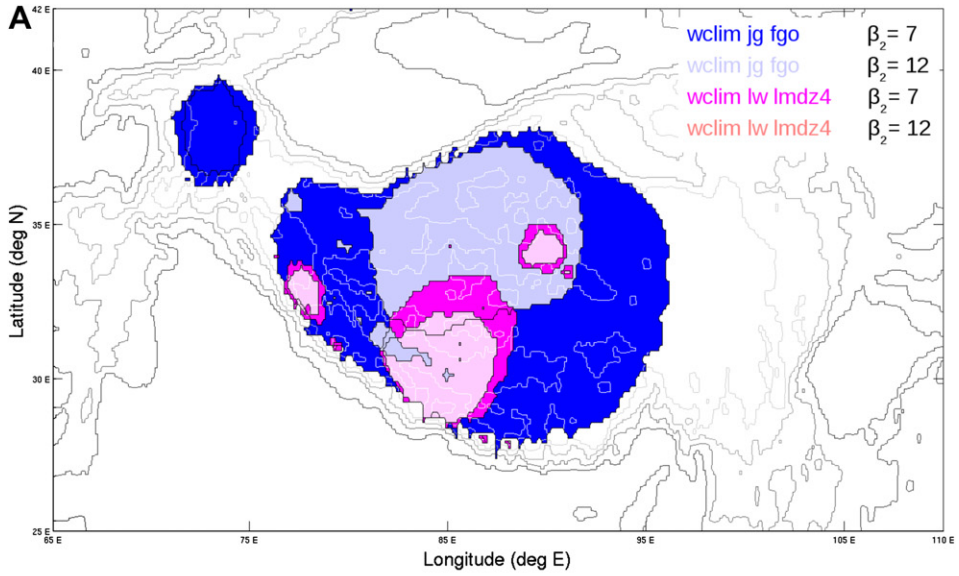

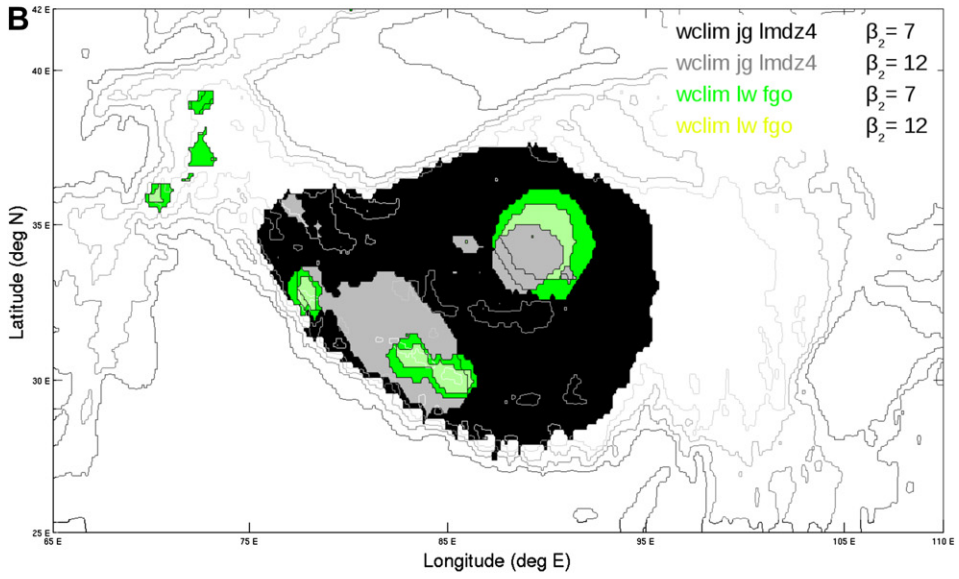

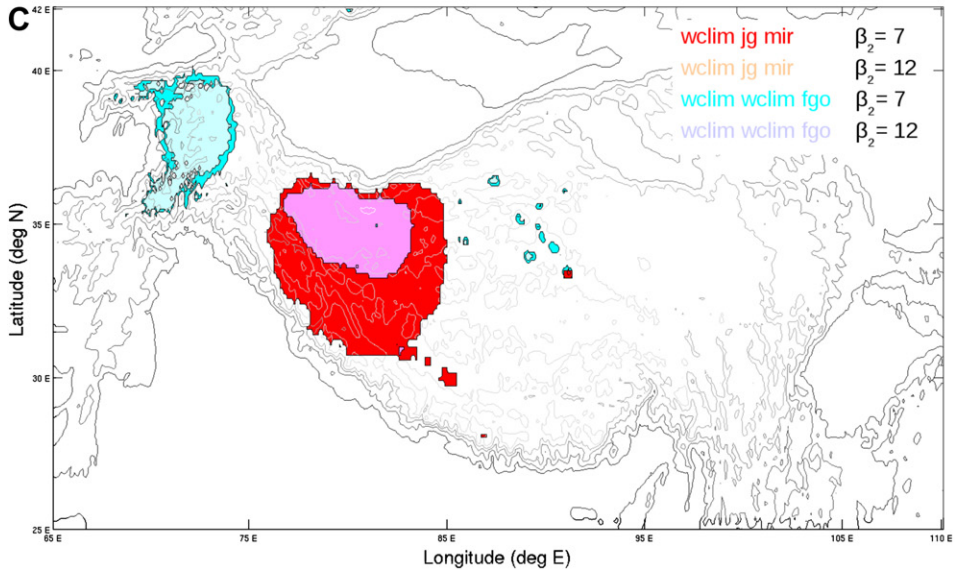

Please cite this article in press as: Kirchner, N., et al., Paleoglaciological reconstructions for the Tibetan Plateau during the last glacial cycle:..., Quaternary Science Reviews (2010), doi:10.1016/j.quascirev.2010.11.006

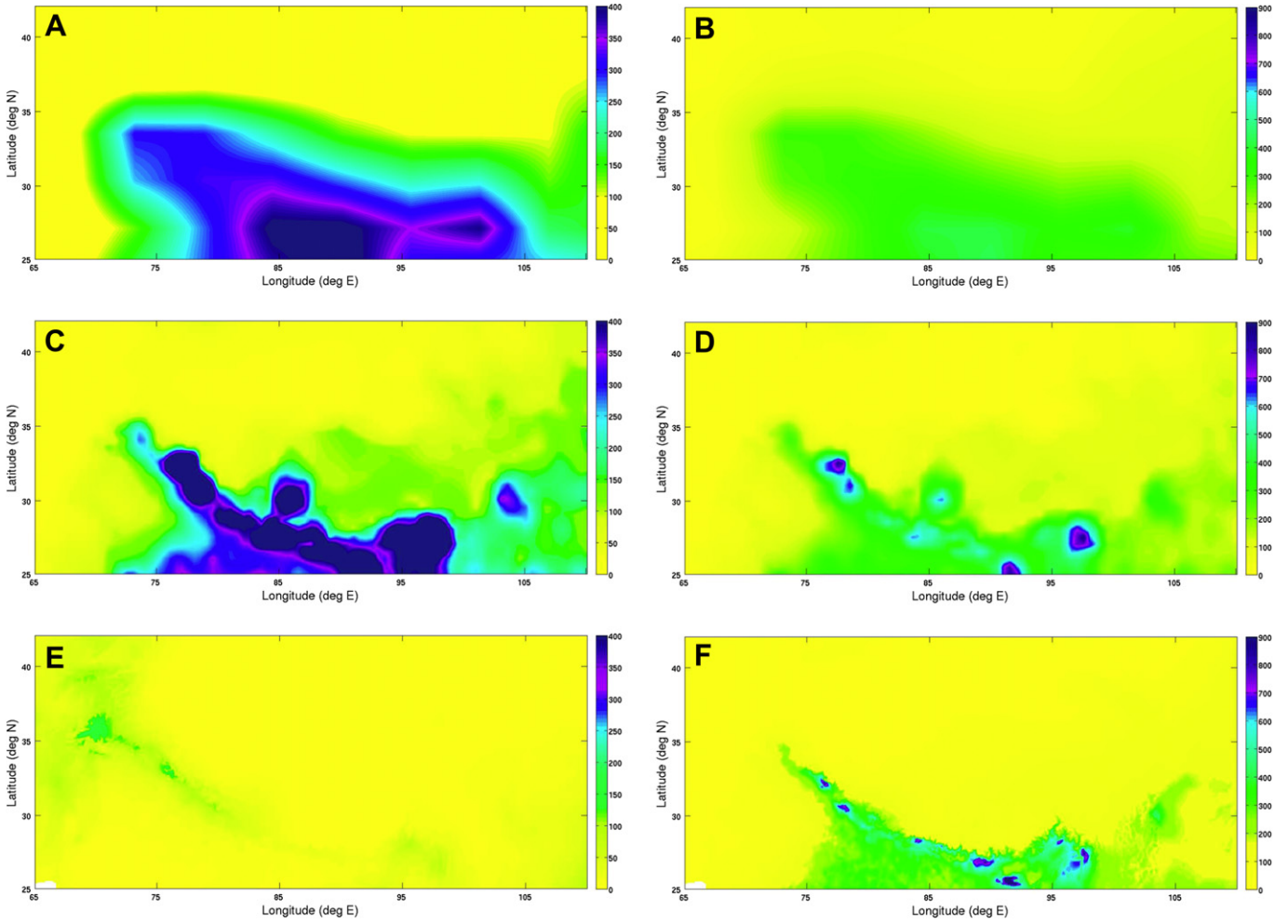

Fig. A2. Illustration of the contemporary precipitation data sets used to force SICOPOLIS. (A) Contemporary February mean precipitation (in mm water equivalent per month) over the Tibetan Plateau as derived from the ECMWF data set. (B) Contemporary August mean precipitation over the Tibetan Plateau as derived from the ECMWF data set. (C) Contemporary February mean precipitation over the Tibetan Plateau as derived from the Legates & Willmott data set. (D) Contemporary August mean precipitation over the Tibetan Plateau as derived from the Legates & Willmott data set. (E) Contemporary February mean precipitation over the Tibetan Plateau as derived from the WorldClim data set. (F) Contemporary August mean precipitation over the Tibetan Plateau as derived from the WorldClim data set, see Appendix A.

Owen, 2005). In addition to the mismatch with the geological field evidence, the spatial and temporal patterns of individual model output differ considerably from each other. The spread of the modeled ice extents ranges from ice-free conditions to a plateau-wide ice sheet, and follows no common pattern as to where nuclei of glaciations are located. The inter-model spread is indeed so large that a comparison of the model mean to the geological record is considered meaningless.

Because of the design of the numerical experiments (employing a stand-alone ice sheet model in which feedback processes with the atmosphere, for example, are included only in a simplified manner despite the fact that Asian Monsoon variability or stationary atmospheric waves will significantly affect precipitation patterns over the Tibetan Plateau), the climate forcing and the glacial index are expected to have the largest impact on the evolution of modeled ice masses. While differences in the employed GCM-based forcings reflect current known uncertainties, their effects when used in numerical simulations tailored especially to the Tibetan Plateau remained previously unexplored.

As a result of our study, we can now conclude that the simulations performed here fail to provide meaningful support of available spatial reconstructions of Tibetan Plateau glaciations during the last glacial cycle as neither common spatial nor temporal patterns can be established from the ensemble of climate forcings.

This mismatch can be attributed to several causes. First, the employed grid resolution implies an averaging of topography and climate data over approximately 9 km $\times$ 8 km. While this may be regarded as high resolution for ice sheet modeling, and indeed is higher than in previous glacier models used for the Tibetan Plateau, the restricted extent of past glaciations on the Tibetan Plateau (Fig. 1C) implies that most ice masses will only be represented by a few grid cells.

Second, there are large uncertainties in the present-day climate description for the Tibetan Plateau used as input to the numerical model. The data sets (Figs. A1 and A2) are based on interpolations of data from weather stations and, in particular for the western and central parts of the Tibetan Plateau, the available data is sparse (cf Hijmans et al., 2005). Further, the uncertainty of the interpolated

Fig. 11. Spatial extents and geographical location of extra-large ice volumes (60,000 km^3–3,000,000 km^3) over the Tibetan Plateau at OIS 2 (LGM). (A) Modeled ice extent in response to forcings 'wclim-jg-fgo' and 'wclim-lw-lmdz4'. (B) Modeled ice extent in response to forcings 'wclim-jg-lmdz4' and 'wclim-lw-fgo'. (C) Modeled ice extent in response to forcings 'wclim-jg-mir' and 'wclim-wclim-fgo'. For a comparison of the OIS 2 ice extents to their OIS 4 counterparts, see Fig. 10.

Please cite this article in press as: Kirchner, N., et al., Paleoglaciological reconstructions for the Tibetan Plateau during the last glacial cycle:..., Quaternary Science Reviews (2010), doi:10.1016/j.quascirev.2010.11.006

data is particularly large for high-relief regions which characterize extensive areas of the Tibetan Plateau. The uncertainty in the present-day climate description will necessarily propagate into climate reconstructions.

Third, nine out of ten paleoclimate-reconstructions employed here are based on GCM model output via an anomaly approach coupled to a glacial index function, cf eqns. (3)–(5), whereas the tenth is derived on the basis of the GRIP record, cf the description following eq. (2). While both approaches have been successfully employed in numerical ice sheet modeling experiments set up for Greenland and the ephemeral high-latitude Northern Hemisphere ice sheets, they appear less suited in simulations that specifically focus on the mid-latitude, high-relief Tibetan Plateau. In the case of the GRIP-based paleoglaciological reconstruction, it is instructive to point out that our modeled ice volumes over the Tibetan Plateau match the results obtained earlier by Greve et al. (1999), where such extreme ice volumes were considered an artifact in the context of modeling the deglaciation of the Northern Hemisphere. We have now demonstrated that those spurious ice volumes are a direct consequence of the shortcomings of the paleoclimate forcing when applied to the Tibetan Plateau region and can thus tie what was previously believed to be an artifact to a definite cause – the failure of the GRIP data (as well as the GCM-model data) as proxies for surface air temperatures over the Tibetan Plateau area.

Fourth, the glacial index function employed in the anomaly approach is intended to represent the essential characteristics of global climate change. Hence, processes that are specific to either certain areas and/or certain time periods cannot be resolved. Thus, some shortcomings of the modeling performed for the Tibetan plateau region must be attributed to the glacial index function $g(t)$. The temporal mismatch, in particular, between the model output and the geological evidence, with the model yielding most extensive glaciers during OIS 2, indicate that the GRIP record and the glacial index function do not capture the palaeo-climate history of the Tibetan Plateau. Apparently the glacial climate on the Tibetan Plateau differed to yield smaller ice advances, perhaps through higher aridity. The demonstrated inability to prescribe the Tibetan Plateau paleoclimate with a North Atlantic ice core record coupled to a glacial function supports previous notions that Tibetan Plateau glaciations are controlled by competing atmospheric systems such as the Asian monsoon in the south and the east and the westerlies in the northwest (Benn and Owen, 1998; Owen et al., 2005).

Finally, the sensitivity of the ice sheet model with respect to changes in parameters such as the factor of ice melt in the PDD model has only been partly explored. Eventually, a rigorous sensitivity analysis exploring an entire parameter space, as recently suggested by Stone et al. (2010), should be carried out for the paleosimulations presented here. The infrastructure for Latin hypercube sampling within SICOPOLIS is currently set up.

As a consequence of these limitations, the following ice sheet model shortcomings were identified. First, the ice sheet model failed to match the contemporary glaciation cover over the Tibetan Plateau. In most cases modeled ice extent is too restricted. 30 runs resulted in ice-free conditions and another 14 runs resulted in modeled present-day ice patches that extended over at most five grid cells when plotted (cf Figs. 6, 8 and 10 and 11).

Second, with the reduced ensemble of climate forcings considered here, the ice sheet model yields ice-free conditions at all times on the eastern part of the Tibetan Plateau. This may be an artifact related to grid size averaging procedures or the use of a stand-alone ice sheet model, or a real feature reflecting that typical ice masses are no larger than one grid cell. However, the absence of ice in this area seems to be a result of the climatology used as forcing, because some contemporary ice caps located on the eastern fringe of the Tibetan Plateau appear to have existed there for more than 100 ka (e.g. the Dunde Ice Cap; Thompson et al., 1989).

To arrive at acceptable reconstructions of Tibetan Plateau glaciations during the last glacial cycle using ice sheet modeling, we suggest to analyze the uncertainty in the present-day climatology. This can be achieved by comparing climate forcings stemming from re-analyses of climate datasets such as the ERA-40 data set (Simmons and Gibson, 2000, cf http://www.ecmwf.int/research/era/do/get/era-40), with the purely measurement based climate forcings employed in this study. However, such an analysis has not yet been attempted in the context of Tibetan Plateau paleoglaciological simulations.

Perhaps the most urgent research need concerns the method of reconstructing past climate in long-term ice sheet simulations. This task involves a rigorous analysis of the suitability of the glacial index function over the modeling domain, and, possibly, the modification of the glacial index function if $g(t)$ is considered to be inappropriate. The definition of objective criteria for testing $g(t)$ is very difficult and likely requires the introducing of statistical and/or design-of-experiment methods.

Due to the complexity of the task, progress is achieved only slowly. Until improved methodologies and models become available, long-term coupled simulations with dynamic ice sheet models will continue to depend strongly on the choice of GCM used to reconstruct past climate forcing. They will, consequently, exhibit in their results a variability that is unmatched by the glaciogeological record. This we have shown for the geographical region of the Tibetan Plateau, the glacial history of which we investigated numerically for the time span from −125 ka until present by using a large ensemble of climate forcing derived from the PMIP2 database and other sources (Braconnot et al., 2007; Colleoni, pers. comm. 2009). The divergence of our systematic modeling study provides strong support for Pollard's (2000, p. 104) hypothesis that results of paleoglacial simulations depend 'seriously and probably spuriously' on the climate forcing employed.

5. Conclusions

This is indeed observed, and it is noteworthy that the newer generation GCMs employed in the present study and taken from the PMIP2 database apparently suffer from similar drawbacks as their predecessors in the PMIP1 database. The results of our study are qualitatively contrasted with available spatial reconstructions of Tibetan Plateau glaciations (Li et al., 1991; Fig. 1B). We find that, for the Tibetan Plateau, none of the modeled ice configurations seems to conform to available glacial geological evidence. Hence, we conclude that our results concerning the Tibetan Plateau region are in strong support of the Pollard (2000) findings and thus extend this study in its scope to also include high Asia. Considering the size of the ensemble forcing, this numerical study is one of the most detailed available to test numerical ice sheet modeling over the Tibetan Plateau for predictive power.

(1) Forcing paleoglacial simulations performed with the ice sheet code SICOPOLIS, with a large ensemble of climate forcings derived from the PMIP2 database yields highly diverging results concerning the timing, location and extent of Tibetan Plateau glaciation during the last 125 ka. Extreme end members include an ice-free Tibetan Plateau and a plateau-scale ice sheet, comparable, in size, to the contemporary Greenland ice sheet.
(2) None of the modeled ice configurations conforms with glacial geological evidence when investigated at three key time slices: OIS 4 (−65 ka), OIS 2 (LGM, −21 ka) and today (0 ka).
(3) Numerical simulations that acceptably conform to published reconstructions of Quaternary ice extent on the Tibetan Plateau

Please cite this article in press as: Kirchner, N., et al., Paleoglaciological reconstructions for the Tibetan Plateau during the last glacial cycle:..., Quaternary Science Reviews (2010), doi:10.1016/j.quascirev.2010.11.006

cannot be achieved with a stand-alone ice sheet model when merely forced by paleoclimates derived from currently available GCMs.

(4) We performed a systematic numerical study testing numerical ice sheet modeling over the Tibetan Plateau to probe Pollard's (2000) hypothesis that results of paleoglacial simulations do seriously and probably spuriously depend on the climate forcing employed. The results presented in this study are in strong support of Pollard's (2000) hypothesis. The divergence of the results obtained from the numerical ice sheet modeling provides strong support by itself. However, the comparison of the numerical results to available glacial geological data, emphasizing that none of the modeled ice configurations seems to be correct, provides support to Pollard's (2000) hypothesis in a framework that does not only rely on numerical modeling but rather combines paleoglaciological reconstructions and field evidence.

(5) Whether future ice sheet modeling exercises, incorporating the improvements suggested in Section 4, will succeed in reproducing acceptable reconstructions of Tibetan Plateau glaciations during the last glacial cycle remains an open issue.

Acknowledgements

We acknowledge the international modeling groups for providing their data for analysis and the Laboratoire des Sciences du Climat et de l'Environnement (LSCE) for collecting and archiving the model data within the Paleoclimate Modeling Intercomparison Project PMIP2. The PMIP2 Data Archive is supported by CEA, CNRS, the EU project MOTIF (EVK2-CT-2002-00153) and the Programme National d'Etude de la Dynamique du Climat (PNEDC). The analyses were performed using the database in its version of 10/2008. More information is available on http://pmip2.lsce.ipsl.fr/.

We thank Q. Zhang (Dept of Meteorology, Stockholm University, Sweden) and P. Hancke (Dept of Mechanical Engineering, Darmstadt University, Germany) for invaluable support in pre-processing the PMIP2-data sets for subsequent implementation into SICOPOLIS. The LMDZ4 data set was provided to us by F. Colleoni (LGGE, Grenoble, France), which we gratefully acknowledge.

The simulations were performed on the computing cluster of the Dept of Geological Sciences (DGS) at Stockholm University. We are grateful to M. Jakobsson (DGS) and B. Eriksson (DGS) for granting us access to the cluster and providing valued technical support. We thank R. Mohammed (DGS) and P. Applegate (Dept of Physical Geography and Quaternary Geology, Stockholm University) for supporting the post-processing and visualization of the model results, and P. Applegate moreover for correcting the language. G. Svendsson (Dept of Meteorology, Stockholm University) read an earlier draft of the manuscript; her suggestions and critical remarks were highly beneficial. Finally, we express our sincere thanks to 2 anonymous reviewers whose comments were highly appreciated. This manuscript is a contribution from the Bert Bolin Centre for Climate Research, Stockholm University, Sweden.

Appendix. Present day climatology for the Tibetan Plateau

A.1. Surface air temperature data sets

The three different data sets providing today's surface air temperatures as input to SICOPOLIS are the following:

- The ECMWF data for the years 1986–1989 and 1991–1994, which have already been used in simulations of the deglaciation of the Northern Hemisphere by Greve et al. (1999). This ECMWF data set covers the entire Earth in a spatial resolution of 2.5° × 2.5°, and provides monthly mean temperature values for both midnight and midday.
- The data set of Legates and Willmott (1990a) which contains mean monthly surface air temperatures obtained, compiled and counterchecked from various existing sources covering the time span from 1920 to 1980. The resulting database contains 17,986 independent terrestrial station records and 9655 oceanic records. Land surface records are (due to low station density) reported to be sparse in arid, mountainous, and polar regions. The surface temperature records are interpolated to a 0.5° × 0.5° grid, resulting in 361 × 721 temperature values (beginning at 90°N, 180°W and extending to 90°S, 180°E).
- The WorldClim temperature data set (Hijmans et al., 2005) which contains – among others – monthly surface air temperatures and is compiled from a variety of existing source, restricted, where possible, to records from the 1950–2000 period. The edited and merged WorldClim database contains 24,542 terrestrial station records for mean monthly surface air temperature. The temperature records are interpolated to a 30′ × 30′ grid, resulting in 43,200 × 18,000 data entries beginning at 90°N, 180°W and extending to 60°S, 180°E.

Fig. A1a–f illustrates differences in the temperature data sets by comparing mean contemporary February and mean contemporary august surface air temperatures (plotted in °C) for each data set. It is observed that both the ECMWF data (panels a and b) and the WorldClim data (panels e and f) closely mirror the topography of the Tibetan Plateau, while the data derived from the Legates & Willmott data set (panels c and d) do so only to a restricted extent. While all temperature charts are structurally (i.e., in their spatial patterns as well as in the temperature ranges within these patterns) very similar for all longitudes in their southernmost latitudes, differences manifest themselves northward of the Himalayan mountain range on the Tibetan Plateau. While the ECMWF data and the WorldClim data are by and large alike even on the Tibetan Plateau the monthly temperature distribution obtained from the Legates & Willmott data differs both in overall pattern northward of the Himalayan and in the temperatures, and represents the warmest of all considered climates.

A.2. Precipitation data sets

The three different data sets providing today's precipitation as input to SICOPOLIS are the following:

- The Jaeger (1976) data set, which is the oldest one used in this study. It contains monthly mean precipitation for the entire world based on data observed and collected between 1931 and 1960. Records from 32 different sources have been compiled, however, not all sources cover exactly the same time span. Precipitation values are interpolated to a 5° × 5° grid.
- The data set of Legates and Willmott (1990b), which contains monthly mean precipitation values for the entire world which are compiled from various existing global archives of monthly precipitation. Most of the data collected in these archives were observed between 1920s and 1980s – precipitation values are therefore largely representative of this 60-year period, however, with greater weight to more recent, data-rich years. The edited precipitation database of Legates & Willmott contains 24,635 spatially independent terrestrial station records as well as 2223 spatially independent records over the World's oceans. Adequate spatial coverage is claimed for much of the terrestrial surface, however, it is emphasized that Antarctica, Australia, China, and parts of the Far East are underrepresented in the data set. The precipitation records are

interpolated to a 0.5° × 0.5° grid, resulting in 361 × 721 precipitation values (beginning at 90°N, 180°W and extending to 90°S, 180°E).

- The WorldClim data set (Hijmans et al., 2005), which has been published in 2005 and is the newest data set used in this study. To our knowledge, it is applied in the context of ice sheet modeling for the first time. The data set contains monthly mean precipitation for global *land areas* and has been compiled from a variety of existing sources. Where possible, the data is restricted to records collected between 1950 and 2000 – the edited and merged WorldClim database contains 47554 terrestrial station records. The precipitation values are interpolated to a 30′×30′ grid, resulting in 43,200 × 18,000 data entries beginning at 90°N, 180°W and extending to 60°S, 180°E.

Exemplarily, monthly mean precipitation (in mm water equivalent per month) for the months of February and August are plotted for the three data sets in Fig. A2. It is seen that the WorldClim data provides the driest (February) climate, while the Jaeger data provides the wettest (February) one and differences between those two precipitation sets become less pronounced for the month of August. The precipitation from data set by Legates & Willmott is for the month of February similar to the one obtained from the Jaeger data, and for the month of August to the WorldClim data set. The largest differences are observed for the winter (February) precipitation, while the summer precipitation remains essentially the same with differences stemming mostly from the different resolution of the data.

References

Abe-Ouchi, A., Segawa, T., Saito, F., 2007. Climatic conditions for modelling the Northern Hemisphere ice sheets throughout the ice age cycle. Climate of the Past 3, 423–438.

Alley, R.B., 2000. The Younger Dryas cold interval as viewed from central Greenland. Quaternary Science Reviews 19, 213–226.

An, Z.S., Kutzbach, J.E., Prell, W.E., Porter, S.C., 2001. Evolution of Asian monsoons and phased uplift of the Himalayan plateau since late Miocene times. Nature 441, 62–66.

Armstrong, R., Raup, B., Khalsa, S.J.S., Barry, R., Kargel, J., Helm, C., Kieffer, H., 2009. GLIMS Glacier Database. National Snow and Ice Data Center, Boulder, Colorado USA. Digital media.

Baosheng, L., Zheng, W., Zhang, D.D., 2001. Environment and its changes in the monsoon Sandy region of China during the Late Pleistocene and Holocene. Acta Geographica Sinica 75, 127–137.

Benn, D.I., Owen, L.A., 1998. The role of the Indian summer monsoon and the mid-latitude westerlies in Himalayan glaciation: review and speculative discussion. Journal of the Geological Society London 155, 353–363.

Bintanja, R., van de Wal, R.S.W., Oerlemans, J., 2002. Global ice volume variations through the last glacial cycle simulated by a 3-d ice-dynamical model. Quaternary International 95/96, 11–23.

Boulton, G.S., Dongelmans, P., Punkari, M., Broadgate, M., 2001. Palaeoglaciology of an ice sheet through a glacial cycle: the European ice sheet through the Weichselian. Quaternary Science Reviews 20, 591–625.

Braconnot, P., Otto-Bliesner, B., Harrison, S., Joussaume, S., Peterschmitt, J.-Y., Abe-Ouchi, A., Crucifix, M., Driesschaert, E., Fichefet, T.h., Hewitt, C.D., Kageyama, M., Kitoh, A., Laine, A., Loutre, M.-F., Marti, O., Merkel, U., Ramstein, G., Valdes, P., Weber, S.L., Yu, Y., Zhao, Y., 2007. Results of PMIP2 coupled simulations of the Mid-Holocene and Last Glacial Maximum – Part 1: experiments and large-scale features. Climate of the Past 3 (2), 261–277.

Braithwaite, R.J., 1984. Calculation of degree-days for glacier climate research. Zeitschrift für Gletscherkunde und Glazialgeologie 20, 1–20.

Calov, R., Greve, R., 2005. Correspondence. A semi-analytical solution for the positive-degree day model with stochastic temperature variations. Journal of Glaciology 51 (172), 173–175.

Calov, R., Greve, R., 2006. ISMIP HEINO. Ice Sheet Model Intercomparison Project – Heinrich Event INtercOmparison Available online. http://www.pik-potsdam.de/~calov/heino.html.

Calov, R., Marsiat, I., 1998. Simulations of the Northern Hemisphere through the last glacial-interglacial cycle with a vertically integrated and a three-dimensional thermomechanical ice-sheet model coupled to a climate model. Annals of Glaciology 27, 169–176.

Calov, R., Ganopolski, A., Petoukhov, V., Claussen, M., Brovkin, V., Kubatzki, C., 2005. Transient simulation of the last glacial inception with an atmosphere-ocean-vegetation-ice sheet model: Part II: sensitivity and feedback analysis. Climate Dynamics 24 (6), 563–576.

Calov, R., Greve, R., Abe-Ouchi, A., Bueler, E., Huybrechts, P., Johnson, J.V., Pattyn, F., Pollard, D., Ritz, C., Saito, F., Tarasov, L., 2010. Results from the ice-sheet model intercomparison project – Heinrich Event INter Comparison (ISMIP HEINO). Journal of Glaciology 56 (197), 371–383.

Charbit, S., Ritz, C., Philippon, G., Peyaud, V., Kageyama, M., 2007. Numerical reconstructions of the Northern Hemisphere ice sheets through the last glacial-interglacial cycle. Climate of the Past 3, 15–37.

Chevalier, M.L., Ryerson, F.J., Tapponnier, P., Finkel, R.C., Van Der Woerd, J., Li, H.B., Liu, Q., 2005. Slip-rate measurements on the Karakorum Fault may imply secular variations in fault motion. Science 307, 411–414.

Clark, M.K., Schoenbohm, L.M., Royden, L.H., Whipple, K.X., Burchfiel, B.C., Zhang, X., Tang, W., Wang, E., Chen, L., 2004. Surface uplift, tectonics and erosion of eastern Tibet from large-scale drainage patters. Tectonics 23, 1–20.

Colleoni, F., Krinner, G., Jakobsson, M., 2009. Sensitivity of the Late Saalian (140 kyr BP) and LGM (21 kyr BP) Eurasian ice sheet surface mass balance to vegetation feedbacks. Geophysical Research Letters 36. doi:10.1029/2009GL037200.

Cuffey, K.M., Clow, G.D., 1997. Temperature, accumulation, and ice sheet elevation in central Greenland through the last deglacial transition. Journal of Geophysical Research 102, 26383–26396.

Dahl-Jensen, D., Johnsen, S.J., Hammer, C.U., Clausen, H.B., Jouzel, J., 1993. Past accumulation rates derived from observed annual layers in the GRIP ice core from Summit, central Greenland. In: Peltier, W.R. (Ed.), Ice in the Climate System. Springer, Berlin Heidelberg, Germany, pp. 517–532.

Dansgaard, W., Johnsen, S.J., Clausen, H.B., Dahl-Jensen, D., Gundestrup, N.S., Hammer, C.U., Hvidberg, C.S., Steffensen, J.P., Sveinbjörnsdottir, A.E., Jouzel, J., Bond, G., 1993. Evidence for general instability of past climate from a 250-kyr ice core record. Nature 356 (6434), 218–220.

De Angelis, H., 2007. Glacial geomorphology of the east-central Canadian Arctic. Journal of Maps v2007, 323–341.

Derbyshire, E., Shi, Y.F., Li, J.J., Zheng, B.X., Li, S.J., Wang, J.T., 1991. Quaternary glaciation of Tibet: the geological evidence. Quaternary Science Reviews 10, 485–510.

Dyke, A.S., Andrews, J.T., Clark, P.U., England, J.H., Miller, G.H., Shaw, J., Veillette, J.J., 2002. The Laurentide and Innuitian Ice sheets during the last glacial maximum. Quaternary Science Reviews 21, 9–31.

Dyurgerov, M.B., Meier, M.F., 2005. Glaciers and the Changing Earth System: A 2004 Snapshot, vol. 58. Institute of Arctic and Alpine Research, University of Colorado, Occational Paper. 117 pp.

Forssström, P.-L., Greve, R., 2004. Simulation of the Eurasian ice sheet dynamics during the last glaciation. Global and Planetary Change 42 (1–4), 59–81.

Forssström, P.-L., Sallasmaa, O., Greve, R., Zwinger, T., 2002. Simulation of fast-flow features of the Fennoscandian ice sheet during the Last Glacial Maximum. Annals of Glaciology 37, 383–389.

Fowler, A.C., Larson, D.A., 1978. On the flow of polythermal ice in glaciers. I: model and preliminary analysis. Proceedings of the Royal Society London A 363, 217–242.

Frenzel, B., 1960. Die Vegetations- und Landschaftszonen Nordeurasiens während der letzten Eiszeit und während der Postglazialen Warmzeit. Akademie der Wissenschaften und der Literatur in Mainz. Abhandlungen der Mathematisch-Naturwissenschaftlichen Klasse 13, 937–1099.

Greve, R., Blatter, H., 2009. Dynamics of Ice Sheets and Glaciers. Advances in Geophysical and Environmental Mechanics and Mathematics (AGEM^2. Springer.

Greve, R., Weis, M., Hutter, K., 1998. Paleoclimatic evolution and present conditions of the Greenland ice sheet in the vicinity of Summit: an approach by large-scale modeling. Paleoclimates 2, 133–161.

Greve, R., Wrywoll, K.-H., Eisenhauer, A., 1999. Deglaciation of the Northern Hemisphere at the onset of the Eemian and Holocene. Annals of Glaciology 28, 1–8.

Greve, R., 1997a. A continuum-mechanical formulation for shallow polythermal ice sheets. Philosophical Transactions of the Royal Society London, A 355, 921–974.

Greve, R., 1997b. Application of a polythermal three-dimensional ice sheet model to the Greenland Ice Sheet: response to steady-state and transient climate scenarios. Journal of Climate 10 (5), 901–918.

Greve, R., 2005. Relation of measured basal temperatures and the spatial distribution of the geothermal heat flux for the Greenland Ice Sheet. Annals of Glaciology 42, 424–432.

Greve, R., 2010. Ice Sheet Model SICOPOLIS Online documentation. http://sicopolis.greveweb.net.

Hättestrand, C., 1998. The glacial geomorphology of central and northern Sweden. Swedish Geological Survey Ca 85, 47.

Hewitt, C.D., Mitchell, J.F.B., 1997. Radiative forcing and response of a GCM to ice age boundary conditions: cloud feedback and climate sensitivity. Climate Dynamics 13 (11), 821–834.

Heyman, J., Hättestrand, C., Stroeven, A.P., 2008. Glacial geomorphology of the Bayan Har sector of the NE Tibetan Plateau. Journal of Maps v2008, 42–62.

Heyman, J., Stroeven, A.P., Alexanderson, H., Hättestrand, C., Harbor, J., Li, Y.K., Caffee, M.W., Zhou, L.P., Veres, D., Liu, F., Machiedo, M., 2009. Palaeoglaciation of Bayan Har Shan, northeastern Tibetan Plateau: glacial geology indicates maximum extents limited to ice cap and ice field scales. Journal of Quaternary Science 24, 710–727.

Hijmans, R.J., Cameron, S.E., Parra, J.L., Jones, P.G., Jarvis, A., 2005. Very high resolution interpolated climate surfaces for global land areas. International Journal of Climatology 25, 1965–1978.

Please cite this article in press as: Kirchner, N., et al., Paleoglaciological reconstructions for the Tibetan Plateau during the last glacial cycle:..., Quaternary Science Reviews (2010), doi:10.1016/j.quascirev.2010.11.006

Hourdin, F., Musat, I., Bony, S., Braconnot, P., Codron, F., Dufresne, J.L., Fairhead, L., Filiberti, M.-A., Friedlingstein, Grandpeix, J.-Y., Krinner, G., Levan, P., Li, Z.X., Lott, F., 2006. The LMDZ4 general circulation model: climate performance and sensitivity to parametrized physics with emphasis on tropical convection. Climate Dynamics 27 (7–8), 787–813.

Howell, D., Siegert, M., Dowdeswell, J.A., 1999. Numerical modelling of the Eurasian High Arctic Ice Sheet: an inverse experiment using geological boundary conditions. Glacial Geology and Geomorphology v. http://boris.qub.ac.uk/ggg/papers/full/1999/rp061999/rp06.html.

Hutter, K., 1982. A mathematical model of polythermal glaciers and ice sheets. Geophysical and Astrophysical Fluid Dynamics 21, 201–224.

Hutter, K., 1983. Theoretical Glaciology. D. Reidel Publ. Comp. Terra Scientific Publishing Company, Dordrecht, The Netherlands.

Hutter, K., 1993. Thermo-mechanically coupled ice sheet response. Cold, polythermal, temperate. Journal of Glaciology 39 (131), 65–86.

Huybrechts, P., Payne, A.J., The EISMINT Intercomparison Group, 1996. The EISMINT benchmarks for testing ice-sheet models. Annals of Glaciology 23, 1–12.

Inman, M., 2010. Settling the science on Himalayan glaciers. Nature Reports Climate Change. doi:10.1038/climate.2010.19.

Jaeger, L., 1976. Monatskarten des Niederschlags fuer die ganze Erde. Berichte des Deutschen Wetterdienstes 139, 38.

Johnsen, S.J., Dahl-Jensen, D., Dansgaard, W., Gundstrup, N.S., 1995. Greenland paleotemperatures derived from GRIP borehole temperature and ice core isotope profiles. Tellus 47B (5), 624–629.

Kleman, J., Hättestrand, C., 1999. Frozen-bed Fennoscandian and Laurentide ice sheets during the Last Glacial Maximum. Nature 402, 63–66.

Kleman, J., Hättestrand, C., Borgström, I., Stroeven, A.P., 1997. Fennoscandian palaeoglaciology reconstructed using a glacial geological inversion model. Journal of Glaciology 43, 283–299.

Kleman, J., Fastook, J., Stroeven, A.P., 2002. Geologically and geomorphologically-constrained numerical model of Laurentide Ice Sheet inception and build-up. Quaternary International 95–96, 87–98.

Kleman, J., Jansson, K., De Angelis, H., Stroeven, A.P., Hättestrand, C., Alm, G., Glasser, N., 2010. North American ice sheet build-up during the last glacial cycle, 115–21 kyr. Quaternary Science Reviews 29, 2036–2051.

Knies, J., Kleiber, H.-P., Matthiessen, J., Müller, C., Nowaczyk, N., 2001. Marine ice-rafted debris records constrain maximum extent of Saalian and Weichselian ice-sheets along the northern Eurasian margin. Global and Planetary Change 31, 45–64.

Krinner, G., Boucher, O., Balkanski, Y., 2006. Ice-free glacial northern Asia due to dust deposition on snow. Climate Dynamics 27 (6), 613–625.

Kuhle, M., Herterich, K., Calov, R., 1989. On the ice age glaciation of the Tibetan highlands and its transformation into a 3-D model. GeoJournal 19, 201–206.

Kuhle, M., 1985. Glaciation research in the Himalayas: a new ice age theory. Universitas 27, 281–294.

Kuhle, M., 1998. Reconstruction of the 2.4 million km^2 late Pleistocene ice sheet on the Tibetan Plateau and its impact on the global climate. Quaternary International 45/46, 71–108.

Kuhle, M., 2004. The high glacial (Last Ice Age and LGM) ice cover in high and Central Asia. In: Ehlers, J., Gibbard, P.L. (Eds.), Development in Quaternary Science 2c (Quaternary Glaciation – Extent and Chronology, Part III: South America, Asia, Africa, Australia, Antarctica. Elsevier Amsterdam, pp. 175–199.

Kuhle, M., 2007. The past valley glacier network in the Himalayas and the Tibetan ice sheet during the last glacial period and its glacial-isostatic, eustatic and climatic consequences. Tectonophysics 445, 116–144.

Legates, D.R., Willmott, C.J., 1990a. Mean seasonal and spatial variability in global surface air temperature. Theoretical and Applied Climatology 41, 11–21.

Legates, D.R., Willmott, C.J., 1990b. Mean seasonal and spatial variability in gauge-corrected, global precipitation. International Journal of Climatology 10, 111–127.

Lehmkuhl, F., Owen, L.A., 2005. Late Quaternary glaciation of Tibet and the bordering mountains: a review. Boreas 34, 87–100.

Lehmkuhl, F., 1998. Extent and spatial distribution of Pleistocene glaciations in eastern Tibet. Quaternary International 45/46, 123–134.

Li, B., Li, J., Cui, Z. (Eds.), 1991. Quaternary Glacial Distribution Map of Qinghai-Xizang (Tibet) Plateau 1:3,000 000. Scientific advisor: Shi Yafeng, Quaternary Glacier and Environment Research Center, Lanzhou University.

Lindvall, J., 2009. Atmosphere-ice sheet interaction through stationary waves. Master's thesis. Department of Meteorology, Stockholm University; 2009.

Mangerud, J., Dokken, T., Hebbeln, D., Hehhen, B., Ingolfsson, O., Landvik, J.Y., Mejdahl, V., Svendsen, J.I., Vorren, T.O., 1998. Fluctuations of the Svalbard-Barents Sea Ice sheet during the last 150,000 years. Quaternary Science Reviews 17, 11–42.

Marsiat, I., 1994. Simulation of the Northern Hemisphere continental ice sheets over the last glacial–interglacial cycle: experiments with a latitude-longitude vertically integrated ice sheet model coupled to a zonally averaged climate model. Paleoclimates 1, 59–98.

Molnar, P., England, P., 1990. Late Cenozoic uplift of mountain ranges and global climate change. Chicken or egg? Nature 346, 29–34.

Moren, B., Heyman, J., Stroeven, A.P., in review. Glacial geomorphology of the central Tibetan Plateau. Journal of Maps.

Morland, L.W., 1984. Thermo-mechanical balances of ice sheet flows. Geophysical and Astrophysical Fluid Dynamics 29, 237–266.

Napieralski, J., Hubbard, A., Li, Y.K., Harbor, J., Stroeven, A.P., Kleman, J., Alm, G., Jansson, K.N., 2007. Towards a GIS assessment of numerical ice sheet model performance using geomorphological data. Journal of Glaciology 42, 135–144.

Owen, L.A., Benn, D.I., 2005. Equilibrium-line altitudes of the Last Glacial Maximum for the Himalaya and Tibet: an assessment and evaluation of results. Quaternary International 138–139, 55–78.

Owen, L.A., Finkel, R.C., Barnard, P.L., Ma, H.Z., Asahi, K., Caffee, M.W., Derbyshire, E., 2005. Climatic and topographic controls on the style and timing of Late Quaternary glaciation throughout Tibet and the Himalaya defined by 10Be cosmogenic radionuclide surface exposure dating. Quaternary Science Reviews 24, 1391–1411.

Owen, L.A., Caffee, M.W., Bovard, K.R., Finkel, R.C., Sharma, M.C., 2006a. Terrestrial cosmogenic nuclide surface exposure dating of the oldest glacial successions in the Himalayan orogen: Ladakh Range, northern India. Geological Society of America Bulletin 118, 383–392.

Owen, L.A., Finkel, R.C., Ma, H.Z., Barnard, P.L., 2006b. Late Quaternary landscape evolution in the Kunlun Mountains and Qaidam basin, northern Tibet: a framework for examining the links between glaciation, lake level changes and alluvial fan formation. Quaternary International 154–155, 73–86.

Owen, L.A., Caffee, M.W., Finkel, R.C., Seong, Y.B., 2008. Quaternary glaciation of the Himalayan-Tibetan orogen. Journal of Quaternary Science 23, 513–531.

Owen, L.A., Robinson, R., Benn, D.I., Finkel, R.C., Davis, N.K., Yi, C.L., Putkonen, J., Li, D.W., Murray, A.S., 2009. Quaternary glaciation of Mount Everest. Quaternary Science Reviews 28, 1412–1433.

Owen, L.A., Yi, C.L., Finkel, R.C., Davis, N.K., 2010. Quaternary glaciation of Gurla Mandhata (Naimon anyi). Quaternary Science Reviews 29, 1817–1830.

Petit, J.R., 18 others, 1999. Climate and atmospheric history of the past 420,000 years from the Vostok ice core, Antarctica. Nature 399, 429–436.

Pollard, D., PMIP Participating Groups, 2000. Comparisons of ice-sheet surface mass budgets from Paleoclimate Modeling Intercomparison project (PMIP) simulations. Global and Planetary Change 24, 79–106.

Ramstein, G., Fluteau, F., Besse, J., Joussaume, S., 1997. Effect of orogeny, plate motion and land-sea distribution on Eurasian climate change over the past 30 million years. Nature 386, 788–795.

Raymo, M.E., Ruddiman, W.F., 1992. Tectonic forcing of late Cenozoic climate. Nature 359, 117–122.

Reeh, N., 1991. Parameterization of melt rate and surface temperature on the Greenland ice sheet. Polarforschung 59 (3), 114–128.

Roe, G.H., Lindzen, R.S., 2001. The mutual interaction between continental-scale ice sheets and atmospheric stationary waves. Journal of Climate 14 (7), 1450–1465.

Rutter, N., 1995. Problematic ice sheets. Quaternary International 28, 19–37.

Schäfer, J.M., Tschudi, S., Zhao, Z.Z., Wu, X.H., Ivy-Ochs, S., Wieler, R., Baur, H., Kubik, P.W., Schlüchter, C., 2002. The limited influence of glaciations in Tibet on global climate over the past 170,000 yr. Earth and Planetary Science Letters 194, 287–297.

Schäfer, J.M., Oberholzer, P., Zhao, Z.Z., Ivy-Ochs, S., Wieler, R., Baur, H., Kubik, P.W., Schlüchter, C., 2008. Cosmogenic beryllium-10 and neon-21 dating of late Pleistocene glaciations in Nyalam, monsoonal Himalayas. Quaternary Science Reviews 27, 295–311.

Seong, Y.B., Owen, L.A., Yi, C.L., Finkel, R.C., 2009. Quaternary glaciation of Muztag Ata and Kongur Shan: evidence for glacier response to rapid climate changes throughout the late glacial and Holocene in westernmost Tibet. Geological Society of America Bulletin 121, 348–365.

Shi, Y.F., Zheng, B.X., Li, S.J., 1992. Last glaciation and maximum glaciation in the Qinghai-Xizang (Tibet) Plateau: a controversy to M. Kuhle's ice sheet hypothesis. Zeitschrift fi Geomorphologie NF Supplementband 84, 19–35.

Simmons, A.J., Gibson, J.K., 2000. The ERA-40 Project Plan. In: ERA-40 Project Report Series, vol. 1. European Center for Medium Range Weather Forecast ECMWF, 63 pp.

Stone, E.J., Lunt, D.J., Rutt, I.C., Hanna, E., 2010. The effect of more realistic forcings and boundary conditions on the modelled geometry and sensitivity of the Greenland ice-sheet. The Cryosphere Discuss 4, 233–285.

Stroeven, A.P., Hättestrand, C., Heyman, J., Harbor, J., Li, Y.K., Zhou, L.P., Caffee, M.W., Alexanderson, H., Kleman, J., Ma, H.Z., Liu, G.N., 2009. Landscape analysis of the Huang He headwaters, NE Tibetan Plateau - patterns of glacial and fluvial erosion. Geomorphology 103, 212–226.

Svendsen, J.I., Alexanderson, H., Astakhov, V.I., Demodov, I., Dowdeswell, J.A., Funder, S., Gataullin, V., Henriksen, M., Hjort, C., Houmark-Nielsen, M., Hubberten, H.W., Ingolfson, O., Jakobsson, M., Kjaer, K., Larsen, E., Lokrantz, H., Lunkka, J.P., Lyså, A., Mangerud, J., Maslenikova, O., Matioushkov, A., Murray, A., Möller, P., Niessen, F., Saarnisto, M., Siegert, C., Stein, R., Siegert, M.J., Spielhagen, R., 2004. Late Quaternary ice sheet history of northern Eurasia. Quaternary Science Reviews 23, 1229–1271.

Thompson, L.G., Mosley-Tompson, E., Davis, M.E., Bolzan, J.F., daiJ, KleinL, Yao, T., Wu, X., Xie, Z., Gunestrup, N., 1989. Holocene-late Pleistocene climatic ice core records from Qinghai-Tibetan Plateau. Science 246, 474–477.

U.S. Department of Commerce, National Oceanic and Atmospheric Administration (NOAA), National Geophysical Data Center, 2006. 2-Minute Gridded Global Relief Data (ETOPO2v2). http://www.ngdc.noaa.gov/mgg/fliers/06mgg01.html.

Wu, Z., 1981. Approach to the genesis of the Taklamakan desert. Acta Geographica Sinica 36, 280–291.

Yang, X., 2000. Landscape evolution and precipitation changes in the Badain Jaran Desert during the last 30,000 years. Chinese Science Bulletin 45 (11), 1042–1047.

Please cite this article in press as: Kirchner, N., et al., Paleoglaciological reconstructions for the Tibetan Plateau during the last glacial cycle:..., Quaternary Science Reviews (2010), doi:10.1016/j.quascirev.2010.11.006

Zhang, Y., Liu, S., Ding, Y., 2006. Observed degree-day factoirs and their spatial variation on glaciers in western China. Annals of Glaciology 43, 301–306.

Zheng, B.X., Rutter, N., 1998. On the problem of Quaternary glaciations, and the extent and patterns of Pleistocene ice cover in the Qinghai-Xizang (Tibet) Plateau. Quaternary International 45/46, 109–122.

Zhou, S.Z., Li, J.J., Zhang, S.Q., Zhao, J.D., Cui, J.X., 2004. Quaternary glaciations in China. In: Ehlers, J., Gibbard, P.L. (Eds.), Development in Quaternary Science 2c (Quaternary Glaciation – Extent and Chronology, Part III: South America, Asia, Africa, Australia, Antarctica. Elsevier Amsterdam, pp. 105–113.

Please cite this article in press as: Kirchner, N., et al., Paleoglaciological reconstructions for the Tibetan Plateau during the last glacial cycle:..., Quaternary Science Reviews (2010), doi:10.1016/j.quascirev.2010.11.006